Institute of Parasitology, Biology Centre CAS
Folia Parasitologica 2021, 68: 012
doi: 10.14411/fp.2021.012

Folia Parasitologica
http://folia.paru.cas.cz

Research Article OPEN ACCESS

Synopsis of the species of *Myxobolus* (Cnidaria, Myxozoa, Myxosporea) described between 2014 and 2020

Jorge C. Eiras[1,2], **Cristina F. Cruz**[1,2], **Aurélia Saraiva**[1,2] and **Edson A. Adriano**[3]

[1] Departamento de Biologia, Faculdade de Ciências, Universidade do Porto, Porto, Portugal;

[2] CIIMAR – Centro Interdisciplinar de Investigação Marinha e Ambiental, Matosinhos, Portugal;

[3] Departamento de Ecologia e Biologia Evolutiva, Universidade Federal de São Paulo – UNIFESP, Diadema, SP, Brazil

Abstract: A synopsis of the species of *Myxobolus* Bütschli, 1882 (Cnidaria, Myxosporea, Myxobolidae) described from 2014 up till now is presented. It includes 122 nominal species described all over the world. For each of the species, the most relevant morphological and morphometric data, as well as data are provided related to the location in the host, type host and type locality. The GenBank accession numbers are provided whenever possible, and the spores were redrawn based on the original descriptions. The bibliography includes all the papers containing the species descriptions.

Keywords: Endocnidozoa, taxonomy, fish parasite, diversity

The genus *Myxobolus* Bütschli, 1882 is between the most diversified Cnidaria of the class Myxozoa. They are mainly fish parasites and have a huge number of different host species, both freshwater and marine ones. Besides *Myxobolus cerebralis* (Hofer, 1903), causing the well-known whirling disease, some other species of *Myxobolus* have also proved to be pathogenic to their hosts (Camus and Griffin 2010, Kaur et al. 2015). Eiras et al. (2005, 2014) published two synopses of *Myxobolus*, which together attained 856 valid species. These papers proved to be useful for researchers interested in the group as judged by the high number of citations they reached – some 358 according to ResearchGate or 399 according to Google Scholar. Driven by the wide acceptance of this type of synopsis by the scientific community of the area, this paper has as aim to compilate the species of *Myxobolus* described from 2014 to date. The authors hope the present compilation is a useful tool for the researchers interested in this interesting group of parasites.

MATERIALS AND METHODS

The present list is based on an extensive internet search, as complete as possible, to detect all the species described since 2014. The authors recognise that, despite their efforts, some species were probably inadvertently overlooked, especially those in papers published in local journals, but hope that such omissions have been kept to a minimum.

The data are organised in tabulated format including the species name, authority, type host and type locality whenever possible, location in the host, description of vegetative stages and spores, including dimensions, and GenBank accession numbers when available.

Spores were re-drawn from the original illustrations, but some were not presented to scale as appeared in the original publications. A complete reference list including all the papers containing the species descriptions is presented. Fish names in Table 1 follow FishBase (Froese and Pauly 2019).

RESULTS

Our literature search resulted in 122 species of *Myxobolus*, which are distributed in all continents, except the Antarctic.

The species features, as mentioned in Materials and Methods, are reported in Table 1 and the drawings of the spores are presented in Figs 1–121. The exception is *Myxobolus bragantinus* Cardim, Silva, Hamoy, Matos et Abrunhosa, 2018, which was not illustrated in the original description.

DISCUSSION

Eiras et al. (2005, 2014) provided previous synopses of species of *Myxobolus*. Until 2005, there were 744 nominal species, and nine years later 112 species had been added, attaining a total number of 856 nominal species (Eiras et al. 2014). The new synopsis here presented shows the addition of 122 species to the genus *Myxobolus*, totaling now 979 taxa. It is interesting to note that, compared with the period covered by the last synopsis (Eiras et al. 2014), the present one shows an increase of 65% in the mean annual

Address for correspondence: Edson A. Adriano, Universidade Federal de São Paulo, Rua Artur Riedel, 275, CEP 09972-270, Diadema, São Paulo, Brasil. Email: edapadriano@gmail.com

number of description of new species. In the first synopsis, there was a mean of 12.4 new species/year (112 species/nine years), while now there is an increase to 20.5 species/year (122 species/seven years). This increase in the pace of description of species suggests that there is still an undescribed diversity of species of *Myxobolus* to be revealed, and the success in this task will depend on the amount of researchers involved in this research area.

Concerning the 122 species presented in this synopsis, it is important to note that almost half (47%) were reported from two country – i.e., India with 35 species and Brazil with 23. This is probably due to two facts: (i) the diversity of fishes is very high in both countries, and (ii) there are several research groups well-established and involved in prospecting myxosporean diversity. Therefore, it cannot be concluded that *Myxobolus* spp. are more abundant (in relative terms considering the number of fish species within a country) if a similar research effort were done in some other countries with high fish diversity.

Another question relates with the habitat of the host fish species. The great majority of new taxa are from freshwater or, at least, were captured in a freshwater environment. We think that this does not necessarily means that *Myxobolus* spp. are more abundant in freshwater. The increase in parasitological studies of marine fish shall demonstrate in the future whether this assumption is correct.

Acknowledgements. The authors are grateful to several colleagues who provided some of the species descriptions: A. Chandran, R. Abdel-Gaber, Bing-Wen Xi, H. Sato, Anabela Costa, C. Antunes, S. Ghosh, Kálmán Molnár, T.G. Rosser, D. Vieira, A. Gupta, E. Kato, Stephen Atkinson, Jan Lovy, J.M. Liu, Juliana Naldoni, Istiyaq Ahmad, Naireen Fariya, Paula Marcotegui, Harpreet Kaur, J. Stilwell. Participation of J.C. Eiras, A. Saraiva and C. Cruz in this study was supported by national funds through FCT – Foundation for Science and Technology within the scope of UIDB/04423/2020 and UIDP/04423/2020.

Table 1. Features of *Myxobolus* spp. described between 2014 and 2020: characteristics of the vegetative stages and spores, type host and type locality, and molecular data when available. Abbreviations: P, vegetative stage; SP, spore; PC, polar capsule; NC, number of coils of the polar filament; IP, intercapsular process; GBAN, Genbank accession number. The dimensions of the spores are indicated as length × thickness × width, and of the polar capsules as length × thickness. All measurements are in micrometres, except those of the vegetative stage that are provided in mm. The host names are those given in the original publications.

Species	Characteristics	Type host and type locality	References
M. adeli Yurakhno et Ovcharenko, 2014	P spindle-shaped, 0.5–1.3, in intestine, pyloric caeca, oesophagus, stomach, swim bladder, sporadically in gills and muscles; SP oval, transversally widened, 6.1 (5.5–6.7) × 7.2 (6.5–7.7) × 4.6 (3.5–5.2); PC equal, 3.0 (2.3–3.8) × 1.8 (1.2–2.2), NC 4. Other localities: Santa Pola Bay, Spain, Black Sea waters (Kerch Channel) and Azov Sea (Genischesk aquatoria – sic); note: the authors did not indicate a type-host or a type-locality. Fig. 1.	*Chelon auratus* (Risso); Ebro River Delta, Spain	Yurakhno and Ovcharenko (2014)
M. adiposus Rocha, Casal, Alves, Antunes, Rodrigues et Azevedo, 2019	P in the adipose tissue surrounding the optic nerve in the ocular cavity, and in urinary bladder; SP spherical, with 12–14 markings near suture line, 9.1 (8.7–9.3) × 9.0 (8.7–9.3); PC pyriform, equal, 4.6 (4.0–5.3) × 3.0 (2.7–3.3), NC 6–7; GBAN: MK 203076. Fig. 2.	*Chelon ramada* (Risso); River Minho (Vila Nova de Cerveira), Portugal	Rocha et al. (2019b)
M. adlardi Gupta et Kaur, 2016	P ovoidal, creamish white, 0.2–0.9, in gill filaments; SP pyriform, ellipsoidal in frontal view, lemon-shaped in sutural view, 7.9 (7.8–8.1) × 4.8 (4.7– 4.9); PC bottle-shaped, equal, 3.5 (3.4– 3.6) × 1.7 (1.6–1.8), NC 6–7. Fig. 3.	*Labeo rohita* (Hamilton); Ranjit Sagar Wetland, Punjab, India	Gupta and Kaur (2016)
M. adrianoi Mathews, Madrid, Martins, Rigoni et Morandini, 2020	In serosa of intestine; SP ellipsoidal, elongated, smooth, up to 22.4 ± 0.3 × 16.3 ± 0.1, in serosa layer of intestine; PC elongated, aubergine-shaped, equal, 14.3 ± 0.2 × 6.5 ± 0.1; NC 5. Fig. 4.	*Corydoras schwartzi* Rössel; Purus River, near Municipality of Labrea, Amazonas state, Brazil	Mathews et al. (2020a)
M. anatolicus Pekmezci, Yardimci, Yilmaz et Polat, 2014	P white, spherical, polysporic, in intralamellar–vascular locations in gills, 0.2 to 1.4 in diameter; SP equal, oval in frontal and sutural views, tapered at anterior pole, 10.1 (9.4–10.7) × 6.9 (6.6–7.2) × 4.5 (4.4–4.6), IP not present; PC pyriform, equal, 4.6 (4.4–4.8) × 2.1 (2–2.3), NC 5–6; GBAN: KF537629. Fig. 5.	*Capoeta tinca* (Heckel); Ondokuzmayıs, Samsun Province, Turkey	Pekmezci et al. (2014)
M. arapiuns Capodifoglio, Meira, Silva, Corrêa, Adriano et Maia, 2020	P rounded, yellow, in pyloric caecum; SP oval in frontal view, fusiform and symmetrical in lateral view, wall smooth with sutural folds, 12.9 (11.6–3.7) × 7.5 (6.8–8.2) × 5.4 (5.1–5.6); PC equal, 5.4 (4.9–6.0) × 2.2 (1.9–2.4), NC 4–5; GBAN: MN239502. Fig. 7.	*Piaractus brachypomus* (Cuvier); Tapajós River, Municipality of Santarém, Pará state, Brazil	Capodifoglio et al. (2020a)
M. arariensis Abrunhosa, Sindeaux-Neto, Santos, Hamoy et Matos, 2018	P whitish, about 1.37 in diameter, in epaxial and hypaxial muscles; SP ellipsoidal, 11.4 (10.7–12.6) × 7.2 (6.4–7.9); PC equal, 4.0 (3.6–4.3) × 1.9 (1.7–2.2); GBAN: MG572219. Fig. 6.	*Rhamdia quelen* (Quoy et Gaimard); Arari River, Cachoeira do Arari in Marajó Island, Brazil	Abrunhosa et al. (2018a)
M. arcasii Rocha, Azevedo, Alves, Antunes et Casal, 2019	P in hematopoietic tissue of kidneys and undifferentiated tissue of gonads; SP subspherical in valvular view and ellipsoidal in sutural view, 6–8 markings near suture line, 9.7 (9.3–10.7) × 8.1 (8.0–8.7) × 6.5 (6.3–6.7); PC pyriform, equal, 3.9 (3.3–4.3) × 3.0 (2.7–3.3), NC 6 (rarely 7); GBAN: MK 053784. Fig. 8.	*Achondrostoma arcasii* (Steindachner); River Minho (Vila Nova de Cerveira), Portugal	Rocha et al. (2019a)
M. arrabonensis Cech, Borzák, Molnár et Székely, 2015	P elongated, 1.0–1.5, inside afferent artery of central and distal part of gill filaments; SP ellipsoidal or shortly ellipsoidal in frontal view, lemon-shaped in sutural view, sutural extensions present, about 0.6 at anterior and 1 at posterior pole of spores, 8.7 (8.4–10.0) × 7.8 (7.6–8.0) × 5.5 (5.4–5.6); PC pyriform, subequal in size, 4.8 (4.5–5.9) × 2.9 (2.7–3.1), NC 6; IP triangular, 1.5 (1.3–1.9) long; GBAN: KP025680–KP025683. Fig. 9.	*Chondrostoma nasus* (Linnaeus); River Danube at Győr, Hungary	Cech et al. (2015)

M. atkinsoni Gupta et Kaur, 2018	P in gills (intralamellar vascular type), 0.5–0.4 in size; SP oblong to oval shaped in valvular view, elliptical in sutural view, anterior end truncated, 6–7 parietal markings on posterior margin, 7.4 × 6.8, without IP; PC oval and unequal, the larger 2.9 × 2.4, NC 6–7, the smaller 2.0 × 1.7, NC 5–6; GBAN: KX143867. Fig. 10.	*Labeo rohita* (Hamilton); Ranjit Sagar Wetland, Punjab, India	Gupta and Kaur (2018a)
M. awadhii Fariya, Abidi et Chauhan, 2018	P white in gill filaments, 0.28–0.39; SP oval to ellipsoidal in valvular view, lenticular in sutural view, 10.5 (7.7–11.6) × 6.7 (5.7–7.3) × 4.8 (4.4–5.1); PC pyriform, tapered anteriorly, equal, 4.6 (3.7–5.8) × 1.6 (1.1–2.1), NC 5–7. Fig. 11.	*Clarias batrachus* (Linnaeus); Lucknow, Uttar Pradesh, India	Fariya et al. (2018a)
M. axelrodi Camus, Dill, Rosser, Pote et Griffin, 2017	P 0.8–0.9 in the third ventricle of brain and 0.1–0.15 in inner plexiform layer of retina; SP elongate, tear drop, curved and pointed anteriorly, rounded posteriorly, 20.5 (19.0–21.8) × 6.6 (5.7–7.9) × 5.1 (4.8–5.9); PC unequal, the larger 9.9 (8.0–11.2) × 3.8 (3.2–4.8), NC about 15–17, the smaller (stunted) 4.1 (3.5–4.5) × 2.0 (1.8–2.3), NC about 5–6. Fig. 12.	*Paracheirodon axelrodi* (Schultz); fish imported from Brazil to USA	Camus et al. (2017)
M. balatonicus Székely, Molnár et Cech, 2015	P ellipsoidal, 0.6–0.8 × 0.4–0.4 in gill filaments; SP ellipsoidal in frontal view and lemon-shaped in sutural view, sutural protrusion forming a circular rim around spore, emerging about 0.6 to 1.1 over spore surface, 7 distinct sutural edge marks, 10.1–12.2 × 8.8–10.1 × 7.1–7.8; PC equal, slightly converging anteriorly, 4.9–6 × 3–3.7, NC 6; IP large, cuneiform; GBAN: KP205545. Fig. 13.	*Cyprinus carpio* Linnaeus; Lake Balaton, Hungary	Székely et al. (2015a)
M. basuhaldari Székely, Cech, Chaudhary, Borzák, Singh et Molnár, 2015	P large, disporoblastic, roundish, 2–3 × 0.2–04, inside multilayered epithelium of gill filaments; SP ovoidal, bluntly pointed with a small knob at tapered anterior end, 7.3 (6.8–7.8) × 5.5 (5.1–6.2) × 3.7 (3.5–3.8); PC equal, pear shaped, 3.2 (2.9–3.7) × 2.1 (2.0–2.2), NC 5; additional host: *Catla catla*, same locality; GBAN: KM029974 for holotype, and KM 029975 and KM 029976 for paratypes. Fig. 14.	*Labeo rohita* (Hamilton); Parikshitgarh Fish Farm, Meerut, India	Székely et al. (2015b)
M. batalhensis Vieira, Alama-Bermejo, Bartholomew, Abdallah et Azevedo, 2017	P whitish, round, about 2.5 in diameter in liver and 5 in ovaries; SP in ovary elongate, ellipsoidal, 15.2 (14.0–15.4) × 8.5 (8.0–8.7) × 5.2 (5.0–5.2), PC elongate and pyriform, equal, 5.2 (5.0–5.5) × 2.8 (2.6–3.0), NC 6-9; SP in liver elongate and pyriform, equal, 15.3 (14.0–15.5) × 8.3 (8.1–8.5) × 5.0 (4.9–5.0), PC elongate and pyriform, 5.4 (5.3–5.5) × 2.8 (2.8–2.9), NC 6–9; GBAN: MF 361090 (ovary specimens) and MF361091 (liver specimens). Fig. 15.	*Salminus hilarii* Valenciennes; Batalha River, Reginópolis, São Paulo State, Brazil	Vieira et al. (2017)
M. bejeranoi Lövy, Smirnov, Brekhman, Ofek et Lotan, 2018	P in striated muscle of gill filaments base; SP ovoid, 10.8 (9.6–11.8) x 6.8 (5.7–8.6); PC equal or nearly equal, 5.2 (4.1–6.4) × 2.2 (1.5–2.6), NC 3-5; GBAN: MF 401455. Fig. 16.	*Oreochromis aureus* × *Oreochromis niloticus;* fish farm in Beit Shean Valley, Israel	Lövy et al. (2018)
M. bjoerknae Molnár, Székely, Guti et Eszterbauer, 2014	P in connective tissue in cartilaginous arch close to base of gill filaments, 0.24–03 × 0.08–0.13; SP ellipsoidal in frontal view, citric shape in sutural view, 17.4 (16.2–18.4) × 13.1 (11.9–13.9) × 10.5 (10–11), emerging suture evenly surrounding spores forming a rim in frontal view, 0.8 (0.7–0.11); PC drop-like, equal, 6.7 (6.3–7.4) × 4.1 (3.6–4.5), NC 6; stout triangular IP, 2.1 (1.8–2.5); GBAN: KF314823. Fig. 17.	*Blicca bjoerkna* (Linnaeus); Lake Balaton, Hungary	Molnár et al. (2014)
M. bragantinus Cardim, Silva, Hamoy, Matos et Abrunhosa, 2018	P in gill filaments, intrafilamental-epithelial type, elongated, milky white, 0.3 × 0.13; SP spherical in frontal view, 6.2 (5.9–6.3) in diameter; PC pyriform, equal, 2.4 (2.1–2.8) × 1.2 (1.2–1.7); GBAN: MH183025.	*Mugil rubrioculus* Harrison, Nirchio, Oliveira, Ron et Gaviria; Bragança, Pará State, Brazil	Cardim et al. (2018)
M. cerveirensis Rocha, Casal, Alves, Antunes, Rodrigues et Azevedo, 2019	P in intestine; SP ellipsoidal in valvular and sutural view, at least 6 markings around posterior half of suture line, 8.1 (7.7–8.7) × 6.8 (6.7–7.3) × 5.3 (5.0–5.7), PC pyriform, equal, 4.2 (4.0–4.7) × 2.8 (2.3–3.0), NC 4–5; GBAN: MK 203079. Fig. 18.	*Chelon ramada* (Risso); River Minho (Vila Nova de Cerveira), Portugal	Rocha et al. (2019b)
M. chanosi Chandran, Zacharia et Sanil, 2019	P in posterior kidney, spherical 0.056 × 0.051; SP oval with smooth shell valves, 11.0 (9.8–12.0) × 7.7 (7.2–8.5) × 7.6 (7.3–8.1); PC elongate oval, unequal, 6.6 (5. 2–7.5) × 4.6 (3.0–4.1) the larger, and 3.3 (3.1–4.7) × 2.5 (1.5–3.2) the smaller, NC 4 in the larger and 3 in the smaller; GBAN: MK 950863. Fig. 19.	*Chanos chanos* (Forskål); Alappuzha, Southwest coast of India	Chandran et al. (2019)
M. chushi Dar, Kaur et Chishti, 2017	P elongatelly oval, white, 0.5 × 2 in gill lamellae (intralamellar vascular type); SP spherical to ovoidal, up to 9 sutural marks at posterior end, 11.1 (10.6–11.4) × 9.1 (8.8–9.2) × 6; PC drop-like, equal, 4.2 (4.0–4.4) × 2.3 (2.0–2.6); IP absent; GBAN: KU885917. Fig. 20.	*Schizopyge niger* (Heckel); Wullar Lake, Kashmir Himalayas, India	Dar et al. (2017a)
M. cultrati Borzák, Molnár, Cech, Papp, Deák-Paulus et Székely, 2016	P not found; batches of spores located in retina layer of eyes; SP elongate-ellipsoidal in frontal view, 9.8 (9.2–10.4) × 6.4 (6.0–6.8); PC elongate, equal, 4.5 (4.4–4.8) × 2.3 (2.1–2.4), NC not detected; triangular IP, 1.9 (1.6–2.1); GBAN: KU170935. Fig. 21.	*Pelecus cultratus,* (Linnaeus); Lake Balaton, Hungary	Borzák et al. (2016)
M. curimatae Zatti, Naldoni, Silva, Maia et Adriano, 2015	P whitish, ellipsoidal, up to 5 in length in gill filaments; SP round to oval in frontal view and biconvex in lateral view, 13.2 (12–14.7) × 9.7 (7–10.8); PC elongated, equal, 5.2 (4.1–5.8) × 2.5 (1.7–3.9), NC 9–10; GBAN: KP120979. Fig. 22.	*Prochilodus costatus* Valenciennes, São Francisco River, Pirapora City, Minas Gerais State, Brazil	Zatti et al. (2015)
M. danrici Mohilal et Soni, 2017	P not found; SP in gills and intestine, spherical, with rounded posterior and anterior extremities in frontal view, and bi-convex in sutural view, 9.6 (8.1–11.1) × 9.5 (8.1–10.1) × 6.3; prominent V-shaped IP; PC pyriform, equal, 6.4 (5.0–7.1) × 3.7 (3.0–4.0), NC 5–6. Fig. 23.	*Esomus danrica* (Hamilton); Thoubal, Manipur, India	Mohilal and Soni (2017)
M. deformis Fariya, Abidi et Chauhan, 2018	P not observed; SP in gills, shorter than wide, blunt, stout, more or less spherical, dorsoventrally flattened in frontal view, nearly oval or lenticular in sutural view, 7.0 (5.8–7.9) × 9.3 (8.0–10.6); PC unequal, the larger 4.7 (3.8–5.8), the smaller 4.3 (3.2–5.4), NC 3–5. Fig. 24.	*Cyprinus carpio* Linnaeus; Lucknow, Uttar Pradesh, India	Fariya et al. (2018b)
M. dermatoulcerans Stilwell, Stilwell, Camus, Ware, Rosser et Griffin, 2020	P in stratum compactum layer of dermis; SP pyriform, rounded posteriorly, rounded to tapering anteriorly, 16.1 (14.3–16.8) × 8.9 (7.6–10.3) × 6.4 (6.0–6.9); PC slender, elongate, equal, 9.2 (7.4–10.2) × 3.0 (2.1–3.7), NC 11–13; IP absent; GBAN MT912631. Fig. 25.	*Pygocentrus nattereri* Kner; Peru (wild caught, imported into the USA for pet trade)	Stilwell et al. (2020a)

M. dermiscalis Kaur, Attri et Joshi, 2016	P white, round to irregular, in a cavity in scales, 0.5–3.6 in diameter; SP oval to spherical in frontal view, anterior and posterior ends rounded, 5.8–7.8 × 3.9–5.9; PC equal, pyriform, 3.9–5.9 × 1.8–3.8, NC 5–6; IP absent; GBAN: KM092529. Fig. 26.	*Labeo rohita* (Hamilton); Harike Wetland, Punjab, India	Kaur et al. (2016)
M. dibombensis Folefack, Abdel-Baki, Ateba, Fomena et Mansour, 2019	P in fins, ovoid or spherical, of variable sizes, 0.21–0.6 × 0.125–0.41; SP ovoid in frontal view and lenticular in lateral view, with truncated anterior end and rounded posterior one, 6 to 8 valvular folds at posterior end, 16.8 (15.8–18) × 11.4 (10–13); PC ovoid, slightly unequal, 7 (6–8) × 3.6 (3–4), NC 11, the larger, 5.8 (4.8–7) × 3 (2–4), NC 7–9, the smaller; conspicuous IP, 2.9 (2.2–3.8); GBAN: MG737377. Fig. 27.	*Labeobarbus batesii* (Boulenger); N'hole, Cameroon	Folefack et al. (2019)
M. doubleae Milanin, Bartholomew et Atkinson, 2020	P about 1 in diameter, in intrafilamential-epithelial location in gills; SP rounded but compressed in thickness, 11.7 (10.7–12.3) × 8.6 (7.7–9.0) × 5.2 (4.6–5.4); PC pyriform, slightly dissimilar in size, 5.7 (5.1–6.5) × 2.7 (2.4–3.2), NC 8-9; GBAN: seq.1 MK592012, seq. 2 MK5902013. Fig. 28.	*Perca flavescens* (Mitchill), Willamette River, Oregon, USA	Milanin et al. (2020)
M. duriensis Rocha, Azevedo, Alves, Antunes et Casal, 2019	P spherical to subspherical in primary gill filaments; SP subspherical in valvular view and ellipsoidal in sutural view, with smooth valves, 13.5 (13.0–14.0) × 9.0 (8.0–9.7) × 7.6 (7.3–8.0); PC pyriform, equal, 4.9 (4.3–5.3) × 3.4 (3.3–3.7), NC 6; GBAN: MK053783. Fig. 29.	*Pseudochondrostoma duriense* (Coelho); River Minho (Vila Nova de Cerveira), Portugal	Rocha et al. (2019a)
M. elongatum Ghosh et Bandyopadhyay, 2017	P attached to mucous membrane around gill lamellae, 1-2 in size; SP elongated in valvular view, lancet-shaped, valves smooth, 16.2 (13–17.6) × 7.9 (7–9); PC slender and elongated, unequal in size, 8.8 (7–10) × 3.4 (3–4) the larger, and 6.5 (6–7) × 3.4 (3–4) the smaller. Fig. 30.	*Labeo bata* (Hamilton); Garia, South 24 parganas, West Bengal, India	Ghosh and Bandyopadhyay (2017)
M. figueirae Naldoni, Maia, Correa, Silva et Adriano, 2018	P white and spherical, in skin, up to 3 in diameter; SP ovoid in frontal view, biconvex in lateral view, 9.5 (9.1–10) × 6.4 (5.8–6.9) × 4.5 (4.4–4.5); PC unequal in size, 4.1 (3.5–4.6) × 2.1 (1.7–2.6) the larger, and 3.2 (2.4–3.6) × 1.4 (1.2–2.1) the smaller, NC 7–8; GBAN: MG181226. Fig. 31.	*Phractocephalus hemioliopterus* (Bloch et Schneider); Tapajós River, Santarém, Pará State, Brazil	Naldoni et al. (2018)
M. filamentum Naldoni, Zatti, Capodifoglio, Milanin, Maia, Silva et Adriano, 2015	P whitish, elongated, in gill filaments up to 5 in size; SP pear–shaped in frontal view, biconvex in lateral view, with symmetric valves 9.0 (7.5–9.7) × 6.2 (5.2–7.3) × 5.3 (4.8–5.7); PC elongated, equal, 4.7 (3.8–5.5) × 1.7 (1.3–2.2), NC 10–11; GBAN: KJ849240. Fig. 32.	*Brycon orthotaenia* Günther; São Francisco River, Pirapora, Minas Gerais State, Brazil	Naldoni et al. (2015)
M. galaicoportucalensis Rocha, Casa, Alves, Antunes, Rodrigues et Azevedo, 2019	P in intestine; SP ellipsoidal in valvular and sutural view, 12–14 markings near suture line, 11.9 (11.3–12.7) × 10.2 (10.0–10.7) × 6.7 (6.0–9.0); PC pyriform, equal, 4.7 (4.0–5.3) × 2.9 (2.7–3.3), NC 4–5; GBAN: MK203084. Fig. 33.	*Mugil cephalus* Linnaeus; River Minho (Vila Nova de Cerveira), Portugal	Rocha et al. (2019b)
M. ginbuna Kato, Kasai, Tomochi, Li et Sato, 2017	P rounded, 0.16 (0.10–0.19) × 0.12 (0.09–0.16) in intralamellar tissue adjacent to vessels in gill filaments; SP pyriform in valvular view and lemon shaped in sutural view, 12.5 (11.7–13.9) × 9.2 (8.5–9.8) × 7.0 (6.7–7.3); PC pyriform, slightly unequal, 7.2 (6.6–7.6) × 2.9 (2.7–3.2) the larger, and 6.7 (6.1–7.1) × 2.9 (2.4–3.4) the smaller, NC 8–9; thin rod-like IP extending from inside wall of apex; GBAN: LC228238. Fig. 34.	*Carassius langsdorfii* Temminck et Schlegel; Irakawa (Kudengawa River), Yamaguchi City, Japan	Kato et al. (2017)
M. gomtii Abidi, Fariya et Chauhan, 2016	SP in kidney, ellipsoidal or cylindrical in frontal view, 8.0 (7.2–8.9) × 4.8 (4.0–5.1); PC straight, equal, tapered towards anterior end, 4.1 (3.2–5.4) × 1.5 (1.0–1.9), NC 4-6. Fig. 35.	*Labeo rohita* (Hamilton); Lucknow, Uttar Pradesh, India	Abidi et al. (2016)
M. gutturocola Liu, Zhang et Zhao, 2019	P whitish, oval, round or ellipsoidal, 1.4 × 0.9, out of throat serous surface; SP ellipsoidal, unsymmetrical in frontal view, lemon-like in lateral view, smooth, 12.5 (11.6–13.7) × 8.4 (8.4–10.7) × 7.1 (6.8–7.3); PC pyriform, unequal, the larger 5.7 (4.9–6.4) × 3.6 (3.0–4.1), NC 7–8, the smaller 4.6 (4.0–5.5) × 2.6 (2.1–3.6), NC 4–5; IP v-shaped; GBAN: MF 543857, MF543858 and MF 543859. Fig. 36.	*Hypophthalmichthys molitrix* Valenciennes; Hechuan District, Chongqing, China	Liu et al. (2019a)
M. hardevi Gupta et Kaur, 2020	P. round, in gills, 0.4–0.5; SP rounded, bowl-shaped in frontal view, broad and flattened anterior end and rounded posterior one, 8.9 × 6.2, prominent thickening between polar capsules; PC unequal, round to bottle-shaped, the larger 3.3 × 2.7, the smaller 1.3 × 1.3, NC 5–6 and 2–3 in the larger and smaller, respectively; IP absent. Fig. 37.	*Labeo bata* (Hamilton), Ranjit Sagar Wetland, Punjab, India	Gupta and Kaur (2020)
M. harpreetae Ghosh et Bandyopadhyay, 2017	P small, rounded, white, 1–2 in diameter, attached to mucous membrane around gill lamellae; SP ellipsoidal in frontal view, 13.2 (11.4–13.8) × 6.5 (4.9–7.8); PC unequal, 9.1 (8.7–9.2) × 3.4 (2.9–4.0) the larger, 7.9 (7.6–8.3) × 6.5 (4.9–7.8) the smaller. Fig. 38.	*Labeo bata* (Hamilton); Sonarpur, West Bengal, India	Ghosh and Bandyopadhyay (2017)
M. hepatobiliaris Rocha, Casal, Alves, Antunes, Rodrigues et Azevedo, 2019	P in liver and gall bladder Wall; SP ellipsoidal in valvular and sutural view, 6–8 markings near the suture line, 6.6 (6.0–7.0) × 5.2 (4.7–5.7) × 4.1 (4.0–4.3); PC pyriform, equal, 3.0 (2.7–3.3) × 1.7 (1.7–2.0), NC 4; GBAN: MK203078. Fig. 39.	*Chelon ramada* (Risso); River Minho (Vila Nova de Cerveira), Portugal	Rocha et al. (2019b)
M. hilarii Capodifoglio, Adriano, Milanin, Silva et Maia, 2015	P in kidney, round, up to 0.5; SP round, 11.5 (9.8–13.4) × 11 (9.7–12.4) × 7.6 (6.7–9.0); PC elongated, equal, 6.5 (6.0–7.2) × 4.0 (3.6–5.3), NC 5–7; GBAN: KM403404. Fig. 40.	*Brycon hilarii* (Valenciennes); fish farm, Municipality of Mogi Mirim, São Paulo State, Brazil	Capodifoglio et al. (2015)
M. himalayaensis Ahmed, Ahmad, Dar, Awas, Kaur, Ganai et Shah, 2019	P large, 2–10, creamish, elongated, in blood vessels of gill filaments; SP oval to spherical in frontal view with compressed anterior end and acuminate and broadly rounded posterior end, parietal folds present, 9.64 × 7.06; PC pyriform, equal, 4.89 × 2.70, NC 5–6: IP absent. Fig. 41.	*Schizothorax richardsonii* (Gray); River Poonch, District of Jammu and Kashmir, India	Ahmed et al. (2019)
M. holzerae Gupta et Kaur, 2017	P cylindrical and white, in gill lamellae, 0.5–4 in diameter. SP round to elliptical in valvular view, lemon–shaped in side view, 7.6 (7.6–7.7) × 4.2 (4.1–4.3); PC pear shaped, equal, 2.54 (2.54–2.58) × 1.6 (1.5–1.6), NC 5–6; IA absent; GBAN: KX 757027. Fig. 42.	*Labeo rohita* (Hamilton); Ranjit Sagar Wetland in Punjab, India	Gupta and Kaur (2017a)

M. ictiobus Rosser, Grifin, Quiniou, Alberson, Woodyard, Mischke, Greenway, Wise et Pote, 2016	P round, intralamellar, in gill filaments, 0.148 × 0.122; SP spherical, 13.9 (12.7–14.5) × 12.5 (10.7–13.6) × 12.6 (10.3–14.8); PC pyriform, equal, 6.6 (5.6–7.4) × 4.5 (3.7–4.9), NC 5–6; GBAN: KU232371. Fig. 43.	*Ictiobus bubalus* (Rafinesque); catfish aquaculture pond, Washington County, Mississippi, USA	Rosser et al. 2016
M. iecoris Naldoni, Zatti, Silva, Maia et Adriano, 2019	P in liver, whitish, spherical, < 10 in diameter; SP oval, anterior region aculiform in frontal view, 12.8 (11.4–14.2) × 8.7 (7.7–9.9) × 6.9 (6.5–7.5); PC equal, 5.9 (4.9–7.4) × 3.0 (2.3–3.5), NC 8–9; GBAN: MH500002. Fig. 44.	*Salminus franciscanus* Lima et Britsky; São Francisco River, Minas Gerais State , Brazil	Naldoni et al. (2019)
M. imparfinis Vieira, Tagliavini, Abdallah et Azevedo, 2018	SP in primary and middle third of primary gill filaments developed in afferent branchial artery, round, 7.9 (7.1–8.4) × 5.5 (4.5–6.2) × 3.7 (3.1–4.2); PC unequal, 3.9 (3.4–4.5) × 1.7 (1.4–2.0) the larger, 3.4 (3.1–3.8) × 1.5 (1.2–1.8) the smaller, NC 6–7; GBAN: MF425815 and MF 425816. Fig. 45.	*Imparfinis mirini* Haseman; River Batalha, Agudos, São Paulo State, Brazil	Vieira et al. (2018)
M. indica Saha et Bandyopadhyay, 2017	P whitish, in gill filaments and fins, up to eight per fish, a single P was 0.7–1.1; SP subspherical, with blunt anterior and posterior end in frontal view, 5.8 (5.6–7.2) × 4.1 (3.5–4.9); PC pyriform, equal, 4.1 (3.5–4.9) × 2.7 (1.8–3.5), NC 4–5; small IP. Fig. 46.	*Carassius auratus* Linnaeus; Diamond Harbour, South 24-Parganas, West Bengal, India	Saha and Bandyopadhyay (2017)
M. iquitoensis Mathews, Meertins, Milanin, Espinoza, Flores-Gonzalez, Audebert et Morandini, 2020	P rounded, up to 0.045 in diameter, in distal region of gill filaments; SP ovoid in frontal view, 17.6 (16.2–19.8) × 10.5 (9.8–12); PC elongated, equal, 8.7 (6.9–9.3) × 3.3 (3–3.6); NC 6–7; GBAN: MN995338. Fig. 47.	*Otocinclus cocama* Reis; Yanayacu Brook, Municipality of Jenaro Herrera, Loreto, Peru	Mathews et al. (2020b)
M. jialingensis Gao, Zhang, Yang et Zhao, 2020	A single P, white, oval (3.1 × 2.8) in hepatopancreas of one fish, and a white one, spherical, 3 in diameter, in urinary bladder of other fish; SP (in the urinary bladder with a membraneous sheath) pyriform, 15.8 (15.4–17.0) × 8.0 (7.8–8.9); PC pyriform, unequal, the larger 7.4 (6.7–8.0) × 3.1 (2.8–3.6), the smaller 7.3 (6.6–8.1) × 3.3 (2.9–3.6), NC 7–8; GBAN: MN 066413 (spores from urinary bladder) and MN066414 (hepatopancreas). Fig. 48.	*Tachysurus fulvidraco* (Richardson), Jialing River, Shapingba District, Chongquing, China	Gao et al. (2020)
M. kalavatiae Székely, Cech, Chaudhary, Borzák, Singh et Molnár, 2015	P in gill lamellae, disporoblastic, round, less than 2 mm; SP ellipsoidal both in frontal and sutural view, 7.3 (6.8–7.7) × 5.3 (4.8–5.8) × 3.7 (3.5–3.8); PC pear -shaped, equal, or closely equal, 3.1 (2.9–3.4) × 1.9 (1.6–2.0); GBAN: KM029973. Fig. 49.	*Cirrhinus cirrhosus* (Bloch); Parikshitgarh Fish Farm, Meerut, Uttar Pradesh State, India	Székely et al. (2015b)
M. kashmirensis Dar, Kaur et Chishti, 2017	P minute, round to oval, 0.1–0.3, in gill lamellae; SP pyriform in frontal view, with constriction in neck region, bluntly pointed at anterior end and rounded posteriorly, 9.16 × 3.33; PC pyriform, equal, 3.33 × 0.83, NC 6; IP absent. Fig. 50.	*Schizothorax esocinus* Heckel; Wular Lake, Kashmir, Himalayas, India	Dar et al. (2017b)
M. khaliji Zhang, Al-Quraish et Abdel-Baki, 2014	P whitish, ellipsoidal, or round, 2–4 in diameter, in intestinal wall; SP subspherical to elliptical, sometimes oval in frontal and lateral view, with a prominent thick caudal end, 8.1 (7.2–9.5) × 6.3 (5.1–7.4) × 9.2 (8.3–10.2); PC elliptical, equal, 5.5 (4.1–6.1) × 3.2 (2.1–4.2), NC 3; GBAN: KC711053. Fig. 51.	*Acanthopagrus bifasciatus* (Forsskål); Damman, Saudi Arabia	Zhang et al. (2014)
M. klamathellus Atkinson et Banner, 2017	P swellings 5–10 in size, immediately posterior to host head and on lateral regions of body; SP ovoid, compressed in thickness, 14.3 (13–15) × 9.7 (9.5–10) × 7.7 (7.5–8); PC pyriform, slightly inequal in size, 6.4 (6–7) × 3.8 (3–4), NC 3–5; GBAN: KX261616. Fig. 52.	*Gila coerulea* (Girard); A-canal, Upper Klamath Lake, Oregon, USA	Atkinson and Banner (2017)
M. knobii Kaur et Ahmad, 2017	P minute, round to irregular, white, 0.4 in diameter, attached to gill lamellae; SP oval to spherical, pot-shaped in frontal view, with a prominent anterior knob, shell smooth, 5.8 × 4.2; PC broadly pyriform, equal, 1.9 × 1.7, NC 3–4; IP absent. Fig. 53.	*Cirrhinus mrigala* (Hamilton); Fagan Majra, District of Fatehgarh Sahib, Punjab, India	Kaur and Ahmad (2017)
M. labrosus Rocha, Casa, Alves, Antunes, Rodrigues et Azevedo, 2019	P in urinary bladder; SP oval in valvular view and ellipsoidal in sutural view, about 8 markings near suture line, 10.0 (9.7–10.3) × 8.1 (7.7–8.7) × 5.8 (5.7–6.0); PC pyriform, equal, 4.5 (4.0–5.0) × 2.5 (2.3–2.7), NC 5–7; GBAN: MK203081. Fig. 54.	*Chelon labrosus* (Risso); River Minho (Vila Nova de Cerveira), Portugal	Rocha et al. (2019b)
M. lamellobasis Molnár, Székely, Guti et Eszterbauer, 2014	P in multilayered epithelium of gill filaments close to base of filaments; SP round or roundish, lemon-shaped in sutural view, sutural protrusion in frontal view forming a thick 1.0 (0.9–1.1) circular rim around spore, emerging in sutural view, 1.0 (0.8–1.1) both at anterior and posterior end, 6–8 edge markings clearly seen in sutural rim; 10.1 (9.1–10.8) × 9.7 (8.6–10.5) × 5.5 (5.2–6.1); PC equal, drop-like, 4.7 (4.4–5.0) × 3.3 (2.7 4.8), NC 6; stout, triangular IP, 1.2 (1.0–1.6); GBAN: KF314824. Fig. 55.	*Blicca bjoerkna* (Linnaeus); Lake Balaton, Hungary	Molnár et al. (2014)
M. lepomis Rosser, Baumgartner, Barger et Griffin, 2017	P in edge of primary gill lamellae, elongate-oval, 0.988 × 0.485 (*L. marginatus*) and 0.8 × 0.6 (*Lepomis miniatus* (Jordan)); SP 19.0 (16.8–21.3) × 7.9 (7.0–8.8) × 5.8 (5.3–6.1) in *L. marginatus*, and 18.8 (17.2–20.3) × 8.7 (5.3–6.1) in *L. marginatus*; PC pyriform, equal, 9.0 (8.3–9.8) × 2.5 (2.2–2.7) in *L. marginatus*, and 10.0 (9.2–1.5) × 2.8 (2.2–3.0) in *L. miniatus*, NC 10–12; GBAN: KY203390 and KY203391. Fig. 56.	*Lepomis marginatus* (Holbroock); Big Dand Creek, Big Thicket Natural Preserve in Polk County, Texas, USA	Rosser et al. (2017)
M. lienis Naldoni, Zatti, Silva, Maia et Adriano, 2019	P whitish, spherical, in spleen; SP round to oval in frontal view, biconvex in lateral view, 12.0 (10.3–13.8) × 8.3 (6.8–9.3) × 7.0 (6.0–7.0); PC oval, equal, 4.6 (3.9–5.8) × 2.8 (2.0–3.5), NC 5–6; GBAN: MH 500003. Fig. 57.	*Brycon orthotaenia* Günther; São Francisco River, Pirapra, Minas Gerais State, Brazil	Naldoni et al. (2019)
M. linzhiensis Li, Xi, Zhao et Xie, 2017	P whitish, ovate or ellipsoidal, under epithelium of gill filaments, 1.7 × 0.4; SP suborbicular in frontal view, fusiform shaped in lateral view with tapering anterior, 11.4 (10.1–13.0) × 10.6 (10.0–11.3) × 6.6 (6.2–7.0); PC pyriform with an apophysis at the top end, equal, 5.7 (4.8–6.7) × 3.8 (3.2–4.2), NC 4; GBAN: KY 965935. Fig. 58.	*Schizothorax oconnori* Lloyd; Yarlung Tsangpo River in the Tibetan plateau, China	Li et al. (2017)
M. longissimus Capodifoglio, Adriano, Silva et Maia, 2019	P white, 0.2, biconvex in lateral view, in external wall of stomach, intestine and gill arch; SP 19.1 (18.0–20.0) × 9.4 (8.6–10.4) × 8.3 (7.6–8.9); PC elongated, equal, 10.5 (9.7–11.1) × 2.5 (2.1–2.4), NC 9–10; GBAN: MK032221. Fig. 59.	*Colossoma macropomum* (Cuvier); Tapajós River, Municipality of Santarém, Pará State, Brazil	Capodifoglio et al. (2019)

M. lucknowii Abidi, Fariya, Irshan et Chauhan, 2015	P small, white, embedded in kidney; SP circular in frontal view, lemon-shaped in sutural view, 7.8 (7.1–9.1) × 7.7 (7.0–8.4); PC almost equal in size, 3.7 (3.1–4.1) × 2.2 (2.1–2.6); noticeable IP present. Fig. 60.	*Clarias batrachus* (Linnaeus); Gomti, Lucknow, Uttar Pradesh, India.	Abidi et al. (2015)
M. magai Deli, Folefack et Fomena, 2017	P whitish and ovoid between secondary gill lamellae, 0.17–0.30 × 0.116–0.2; SP ovoid, anterior end larger and hillocky, posterior end narrow, 10.6 (9.0–12.0) × 6.3 (5.5–7.0); PC equal, ovoid, 2.8 (2.4–3.4) × 2.3 (2.0–3.0), NC 4–5. Fig. 61.	*Labeo batesii* Boulenger; Maga, Cameroon	Deli et al. (2017)
M. majraiensis Kaur et Ahmad, 2017	P round to oval, creamish, 0.4 in diameter, attached to gill lamellae; SP egg-shaped in frontal view, ellipsoidal in sutural view, valves smooth, 8.5 × 5.2; PC pyriform, equal, 3.4 × 1.8, NC 5–6; IP absent. Fig. 62.	*Gibelion catla* (Hamilton); Phaagan Majra, District of Fatehgarh Sahib, Punjab, India	Kaur and Ahmad (2017)
M. mapei Georges, Timoléon, Minette et Joseph, 2017	P in liver and kidneys; SP ellipsoidal in frontal view, 13.3 (10.5–16.5) × 6.8 (6–9); PC unequal in size, 6.4 (6–8.2) × 2.8 (2.2–4.5) the larger, 4.1 (3.5–5.2) × 1.6 (1.5–2.2) the smaller; other host: *Enteromius callipterus* (Boulanger) (same sampling place); note: the authors did not indicate a type-host or a type-locality. Fig. 63.	*Oreochromis niloticus* (Linnaeus); Mapé River, Bankim, Adamawa, Cameroon	Georges et al. (2017)
M. marajoensis Abrunhosa, Sindeaux-Neto, Santos, Hamoy et Matos, 2018	P ellipsoidal to oval-shaped, whitish, 0.345 (0.213–0.408) × 0.195 (0.122–0.245) in the muscular layer of the intestine; SP pyriform, 10.9 (10.0–11.6) × 5.1 (4.2–5.4); PC equal, 5.3 ± 0.6 × 1.6 ± 0.3; GBAN: KX857727. Fig. 64.	*Rhamdia quelen* (Quoy et Gaimard), Baracauari River, Salvaterra, Marajó Island, Pará State, Brazil	Abrunhosa et al. (2018b)
M. markiwi Kaur et Ahmad, 2016	P minute, round to oval, creamish, 0.2 in diameter, attached to gill lamellae; SP ovoidal in frontal view, bluntly pointed anteriorly, with prominent knob, smooth, 6.5 (5.6–7.4) × 5.3 (4.3–6.3); PC pyriform, equal, 1.8 (1.2–2.4) × 0.8 (0.3–1.3), NC 4–5, IP absent. Fig. 65.	*Labeo rohita* (Hamilton); Phagan Majra, District Fatehgard Sahib, Punjab, India	Kaur and Ahmad (2016)
M. mauriensis Lovy et Hutcheson, 2016	P in pleural ribs through length of abdominal cavity, surrounded by ossified bone, up to 5 in diameter; SP round or ellipsoidal, 11.1 ± 0.5 × 12 ± 0.5 × 7.8 ± 0.4; PC pyriform, equal, 6.3 ± 0.4 × 4.2 ± 0.3, NC 5–7; IP small or not apparent; GBAN: KU255436; other host and localities: *Alosa pseudoharengus* (Wilson), Great Egg Harbor River and Delaware River, New Jersey, USA. Fig. 66.	*Alosa aestivalis* (Mitchill); Maurice River, New Jersey, USA	Lovy and Hutcheson (2016)
M. marumotoi Li et Sato, 2014	P elongated, reaching more than 4.5 in length, in somatic muscles; SP rounded in valvular view and ovoid in sutural view, 13.8 (13.3–15.0) × 14.6 (14.2–15.0) × 10.8 (10.0–11.7); PC subspherical, 8.4 (7.9–9.6) × 5.9 (5.4–6.3), NC 5–6, IP present; GBAN: AB873007. Fig. 67.	*Odontobutis obscura* (Temminck et Schlegel); Yoshida, Yamaguchi, Japan	Li and Sato (2014)
M. matosi Capodifoglio, Adriano, Silva et Maia, 2019	P in inner surface of operculum, 0.1 SP ellipsoidal in frontal view, biconvex in lateral view, 9.6 (9.1–10.8) × 7.0 (6.5–7.6) × 5.0 (4.6–5.5); PC elongated, equal, 4.3 (3.3–5.0) × 1.9 (1.6–2.2); GBAN: MK032219; note: the authors did not indicate a type-locality. Fig. 68.	*Colossoma macropomun* (Cuvier); Solimões River, Municipality of Manacapuru, Amazonas State, and Tapajós River, Municipality of Santarém, Pará State, Brazil	Capodifoglio et al. (2019)
M. meerutensis Székely, Cech Chaudhary, Borzák, Singh et Molnár, 2015	P small, less than 2 mm, in capillary network of gill lamellae; SP ellipsoidal in frontal view and lemon-shaped in sutural view, sutural protrusion forming a circular rim around spore, emerging about 0.6 to 0.8 on surface of spore, 9.1 (8.8–9.6) × 6.9 (6.4–7.2) × (5.1 (4.9–5.2); small knob-like IP, 0.4–0.5; PC elongated, equal, 4.3 (4.1–4.5) × 2.1 (1.6–2.4), NC 6; GBAN: KM029977. Fig. 69.	*Labeo rohita* (Hamilton); Parikshitgard Fish Farm, Meerut, Uttar Pradesh, India	Székely et al. (2015b)
M. mineirus Naldoni, Carriero, Moreira, Silva, Maia et Adriano, 2020	P. round, in mesentery, about 3.0; SP round in frontal view and biconvex in lateral view, 13.4 (12.8–14.2) × 10.6 (10.0–10.6) × 6.5 (6.0–6.9), valves symmetrical; PC elongated, equal, 5.3 (4.4–6.1) × 3.1 (2.3–3.8), NC 8, GBAN: MT302590. Fig. 70.	*Brycon orthotaenia* Günther; São Francisco River, Pirapora, Minas Gerais State, Brazil	Naldoni et al. (2020a)
M. minutus Rosser, Griffin, Quiniou, Alberson, Woodyard, Mischke, Greenway, Wise et Pote, 2016	P elongate, approximately 1.3 × 0.4, along edge of gill primary lamellae; SP ovoid, 8.8 (7.4–9.6) × 8.8 (7.5–9.9) × 6.7 (6.5–7.3); PC pyriform, equal, 4.3 (3.6–4.9) × 3.3 (2.8–3.8), NC 5–6; GBAN: KU232372. Fig. 71.	*Ictiobus bubalus* (Rafinesque); catfish aquaculture pond, Washington County, Mississippi, USA	Rosser et al. (2016)
M. mucosus Liu, Voronin, Dudin et Zhang, 2016	P white, slightly elongated, oval, 0.3–0.5, in basal subepithelial tissue between gill filaments; SP ellipsoidal in frontal view and lemon-shaped in sutural view, 13.6 (12.8–14.2) × 10.7 (10.3–11.4) × 7.8 (7.2–8.3); PC drop-like, equal in size, 5.5 (4.8–6.0) × 3.6 (3.2–3.8), NC 5–6, distinct stout and triangular IP, 1.6 (1.5–.8) in diameter; GBAN: KP751907, KP751908, KP751909. Other host: *Leuciscus leuciscus* (Linnaeus); note: the authors did not indicate a type-host or a type-locality. Fig. 72.	*Rutilus rutilus* (Linnaeus); Finnish Bay of Baltic Sea and Lake Ladoga, Russia	Liu et al. (2016a)
M. mugiliensis Rocha, Casal, Alves, Antunes, Rodrigues et Azevedo, 2019	P. whitish, subspherical to filamentous, in gill lamellae, 1–2 in length; SP ellipsoidal in valvular and sutural view, 8–10 markings near sutural line, 11.4 (11.0–11.7) × 9.6 (9.0–10.3) × 6.5 (6.0–6.7); PC pyriform, equal, 4.9 (4.7–5.3) × 3.0 (2.7–3.3), NC 5; GBAN: MK203082. Fig. 73.	*Mugil cephalus* Linnaeus; River Minho (Vila Nova de Cerveira), Portugal	Rocha et al. (2019b)
M. muralidharani Ghosh et Bandyopadhyay, 2016	P round, 2–3 in diameter, creamy white, attached to mucous membrane of gill lamellae; SP elongated, smooth, lancet-shaped, 13.8 (13–14) × 5.3 (4.9–6); PC equal, slender, and elongate, 7.3 (6.9–8.0) × 2.5 (1.9–2.9). Fig. 74.	*Labeo rohita* (Hamilton); Hansnkhali of Nadia, West Bengal, India	Ghosh and Bandyopadhyay (2016)
M. muscularis Rocha, Casal, Alves, Antunes, Rodrigues et Azevedo, 2019	P in heart fibers and skeletal muscle; SP oval in valvular view and ellipsoidal in sutural view, 8–10 markings surrounding posterior half of suture line, 9.1 (8.0–10.0) × 7.0 (6.0–8.7) × 5.2 (4.7–6.0); PC pyriform, equal, 4.3 (4.0–5.0) × 2.7 (2.0–3.3), NC 5–6; GBAN: MK203075. Fig. 75.	*Chelon ramada* (Risso); River Minho (Vila Nova de Cerveira) Portugal	Rocha et al. (2019b)
M. nanokiensis Kaur, Katosh, Dar et Singh, 2015	P in gill lamellae, round to ovoid, 0.038–0.040 in diameter; SP pyriform with sharply pointed beak-like in anterior end and rounded in posterior one, 9.2 × 5.7; PC broadly pyriform, equal, 5.7 × 2.7, NC 7–9; IP absent. Fig. 76.	*Labeo rohita* (Hamilton), Patiala (Punjab), India	Kaur et al. (2015)

M. neurofontinalis Ksepka, Rash, Whelan et Bullard, 2019	SP pyriform, intercellular infecting nerve cord and medulla oblongata, having two valves juxtaposed at sutural rim, 13.9 (12.0–16.9) × 9.6 (8.0–12.0) × 8.1 (7.0–10.0), sutural rim with prominent seam, with 0–4 sutural markings; PC clavate, equal or subequal in size, 7.8 (6.0–10.0) × 3.5 (3.0–5.0), NC 7–10; IP 2.3 (1.0–3.0) long by 1.5 (1.0–2.5) wide; GBAN: MN191598. Fig. 77.	*Salvelinus fontinalis* (Mitchill); East Fork South Fork New River, western NC, USA	Ksepka et al. (2019)
M. ngassami Folefack, Defoueng et Fomena, 2017	P whitish between bony rays of fins, operculum, skin and sclera of eye, ovoid or elongated, 0.315 × 0.205; SP ovoid in frontal view, 11.5 (10.7–12.8) × 9.4 (8.3–10.5), 5–6 valvular folds at posterior half of spore; PC ovoid and inequal in length, 50 (4.5–5.6) × 2.8 (2.1–3.4), NC 7–10 the larger, 4.4 (3.5–5.1) × 2.4 (1.7–3) the smaller, NC 5–7, IP 2.3 (2–2.8). Fig. 78.	*Enteromius callipterus* (Boulenger); Sanaga River, Cameroon	Folefack et al. (2017)
M. niger Mathews, Maia et Adriano, 2016	P in serosa layer of gill arch, spherical to ellipsoidal, 0.18 ± 0.01 in diameter; SP elongated to ellipsoidal in frontal view and biconvex in sutural view, 11.3 ± 0.4 × 6.8 ± 0.2 × 4.1 ± 0.2, some aberrant spores with three polar capsules but presenting measurement values of normal spores; PC elongated, equal 5.0 ± 0.3 × 2.0 ± 0.1, NC 6–7. Fig. 79.	*Corydoras melini* Lönnberg et Rendahl; River Negro, near Municipality of Santa Isabel do Rio Negro, Amazonas State, Brazil	Mathews et al. (2016)
M. nigerae Dar, Kaur et Chishti, 2016	P minute, round to ovoid, 0.08–0.1 in diameter, in gills lamellae; SP ovoidal or subspherical in frontal view, 6.6 (6.3–6.9) × 5 (4.8–5.2); PC oval, equal, 3.3 (3.1–3.5) × 1.6 (1.5–1.7), NC 5; IP absent. Fig. 80.	*Schizopyge niger* (Heckel); Wular Lake, Kashmir, India	Dar et al. (2016)
M. nilimae Ghosh et Bandyopadhyay, 2016	P small (1–2), attached to mucous membrane around gill lamellae; SP petal shaped, 16 (15.9–17) × 6.9 (6.2–7.0); PC equal, 10.0 (9.0–11.0) × 3.1 (3.0–3.5), NC 10–12. Fig. 81.	*Labeo rohita* (Hamilton); Tehatta, Nadia, West Bengal, India	Ghosh and Bandyopadhyay (2016)
M. okamurae Gupta et Kaur, 2018	P large, cylindrical, in gills, 5–7 per gill filament, 0.9-3 in diameter; SP pyriform in valvular view, 12.2 × 4.9 in diameter; PC pyriform, equal, 6.1 × 1.4, NC 13.14; prominent intercapsular process present; GBAN: KX146838. Fig. 82.	*Labeo bata* (Hamilton); Ranjit Sagar Wetland, Punjab, India	Gupta and Kaur (2018b)
M. ompok Chaudhary, Goswami, Gupta, Cech, Singh, Molnár, Székely et Sharma, 2018	P in kidney, round, 0.15–0.2 in diameter; SP large, elongated pyriform, both in frontal and sutural views; SP 14.4 (13.6–14.48) × 6.5 (5.6–6.4) × 5.9 (5.2–6.4); PC very elongated, narrowing anteriorly, equal, 8.2 (8.0–8.5) × 1.8 (1.5–2.4), NC 6; IP not present; GBAN: MG760574 and MG760575. Fig. 83.	*Ompok pabda* (Hamilton); Sotiganj, Meerut, *Uttar Pradesh*, India	Chaudhary et al. (2018)
M. oralis Liu, Whipps, Nie et Gu, 2014	P round or ellipsoidal, 2.6–4.0 histozoic in palate; SP obovate in frontal view and lemon-shaped in lateral view, 2–5 V-shaped sutural ridge markings, small proportion of spores (11%) with short tail or much more clearly visible tail (up to 5.2 in length), 11.7 (10.8–12.8) × 8.9 (8.2–9.9) × 6.8 (6.0–7.5); PC pyriform, equal 4.8 (4.0–5.5) ×3.0 (2.9–3.6), NC 5–6; IP small; GBAN: KC315782. Fig. 84.	*Carassius gibelio* (Bloch); Hubei Province, China	Liu et al. (2014)
M. orthotaenae Naldoni, Pereira, Milanin, Adriano, Silva et Maia, 2020	P white and spherical, up to 1.0 in liver; SP ellipsoidal in frontal view, 10.7 (10.0–11.4) × 8.1 (7.3–8.6) × 6.8 (5.3–7.0); PC equal, 4.9 (4.2–5.4) × 2.7 (1.9–2.9), NC 8; GBAN: MN719635. Fig. 85.	*Brycon orthotaenia* Günther; São Francisco River, Municipality of Pirapora, Minas Gerais State, Brazil	Naldoni et al. (2020b)
M. ovarium Naldoni, Pereira, Milanin, Adriano, Silva et Maia, 2020	P spherical, up to 1.0, in surface of ovary; SP oval-shaped in frontal view, 9.8 (9.2–11.0) × 6.5 (5.6–6.9) × 4.9 (4.6–5.0); PC equal, 4.7 (3.9–6.2) × 2.1 (1.8–2.4), NC 8–9; GBAN: MN719638. Fig. 86.	*Brycon orthotaenia* Günther; São Francisco River, Municipality of Pirapora, Minas Gerais State, Brazil	Naldoni et al. (2020b)
M. paksensis Cech, Borzák, Molnár et Székely, 2015	P large, flat, 1.0–1.7, in connective tissue of swim bladder, covered by a thin epithelial layer; SP ellipsoidal in frontal view and lemon-shaped in sutural view, 14.8 (14.4–15.2) × 11 (10.4–12) × 8.7 (8.4–9.2); PC pyriform, equal, 7.0 (6.8–7.6) × 4.3 (4.0–4.6), NC 6; IP relatively small, triangular, 1.6–2.3; GBAN: KP025687–KP025689. Fig. 87.	*Chondrostoma nasus* (Linnaeus); River Danube, Hungary	Cech et al. (2015)
M. parakoi Liu, Zhang, Yang et Zhao, 2019	Single P, white, spherical, 0.23 in gill lamellae; SP elongated, pyriform in frontal view, valves smooth, with pointed anterior end and round posterior one, 15.9 (14.5–17.2) × 7.8 (6.6–9.7); PC pyriform, equal, 8.7 (7.7–9.8) × 3.0 (2.6–3.5), NC 11–12; GBAN: MH196558. Fig. 88.	*Cyprinus carpio* Linnaeus; Jialing River, Shapingba District, Chongqing, China	Liu et al. (2019b)
M. paratoyamai Kato, Kasai, Tomochi, Li et Sato, 2017	P 0.23 × 0.20 and 0.32 × 0.29 in intralamellar tissue adjacent to vessels in gill filaments; SP elongated, pyriform in valvular and sutural views, particularly in valvular view, anterior end slightly bent, 15.4 (14.7–16.4) × 6.3 (5.5–6.8) × 6.1 (5.6–6.4); only one prominent PC functional, the other rudimentary, 6.5 (5.9–7.1) × 3.7 (3.9–4.2), NC 5–6; GBAN: LC228237. Fig. 89.	*Cyprinus carpio* Linnaeus; Irakawa (Kudengawa River, a branch of Fushinogawa River, Yamaguchi City, Japan	Kato et al. (2017)
M. paratypicus Xi, Zhao, Li et Xie, 2019	P oval, in epithelium of gills filaments; SP asymmetric in frontal view and fusiform in sutural view, 13.8 (12.9–14.9) × 9.9 (9.2–11.1) × 7; PC pyriform, unequal, 7.5 (6.2–8.2) × 5.0 (4.2–6) the larger, and 2.7 (2.1–3.6) × 1.4 (1.1–1.9) the smaller, NC 7–8 in the larger; GBAN: MH119080. Fig. 90.	*Hypophthalmichthys molitrix* (Valenciennes); Lake Taihu, Wuxi, China.	Xi et al. (2019)
M. peleci Borzák, Molnár, Cech, Papp, Deák-Paulus et Székely, 2016	P ellipsoidal, 0.6–0.8 × 0.3–0.4, around afferent artery of cartilaginous gill arch; SP round or roundish in frontal view, lemon-shaped in sutural view, mostly with length somewhat greater than width, small knob-like structure 0.7 (0.6–0.8) at anterior end, sutural protrusion in frontal view with thick 0.9 (0.8–1.9) circular rim around spore, in sutural view emerging only slightly over surface of spore and anterior and posterior extremities, 12.1 (11.6–13.2) × 11.4 (10.8–12.5) × 5.8 (5.6–6.0); PC drop-like, equal, 5.5 (5. 2–6.0) × 3.2 (2.8–3.4), NC 4–5; GBAN: KU170934. Fig. 91.	*Pelecus cultratus* (Linnaeus); Lake Balaton, Hungary	Borzák et al. (2016)
M. pelecicola Voronin et Dudin, 2015 It is a junior synonym of *Myxobolus ladogensis* Rumyantsev et Schulman, 1997 (Zhang et al. 2019)	P up to 1.2 in length and 0.1-0.4 in width in skeletal muscles; SP elongate oval, or oval in frontal view, lens-shaped in sutural view, 16.5 (14.9–18.0) × 12.1 (11.6–13.3) × 7.8 (7.4–8.3); PC pyriform, unequal in size, 8.0 (7.5–8.5) × 4.5 (4.2–4.7) the large, 7.6 (7.2–7.8) × 4.0 (3.8–4.3) the smaller, NC 5–6; large but indistinct triangular IP. Fig. 92.	*Pelecus cultratus* (Linnaeus); Finnish Bay and Ladoga Lake, Russia	Voronin and Dudin (2015)

M. peritonaeum Rocha, Casal, Alves, Antunes, Rodrigues et Azevedo, 2019	P yellowish, subspherical to filamentous, attached to visceral peritoneum, 1–2 in length; SP oval in valvular view, 8–10 markings near the suture line, 8.1 (7.7–8.7) × 7.1 (6.7–7.3); PC equal, pyriform, 3.8 (3.3–4.0) × 2.4 (2.0–2.7), NC 4–5; GBAN: MK203080. Fig. 93.	*Chelon labrosus* (Risso); River Minho (Vila Nova de Cerveira), Portugal	Rocha et al. (2019b)
M. petalum Ghosh et Bandyopadhyay, 2017	P round, creamy white, 2–3 in diameter, attached to mucous membrane of gill lamellae; SP oval in valvular view, shell valves smooth, 12.0 (11–13) × 5.9 (5–7); PC slender and elongated, equal, 7.9 (7–8) × 2.9 (2.5–3); filament coils not observed (note: in the camera lucida drawing of PC filament coils are present). Fig. 94.	*Labeo rohita* (Hamilton); Hooghly River, West Bengal, India	Ghosh and Bandyopadhyay (2017)
M. pharyngobranchialis Rocha, Casal, Alves, Antunes, Rodrigues et Azevedo, 2019	P. in denticular pharyngeal pad of pharyngobranchial organ; SP ellipsoidal in valvular and sutural view, 6–8 markings near suture line, 9.3 (8.7–10.0) × 7.7 (7.0–8.0) × 5.8 (4.7–6.0); PC equal, pyriform, 4.7 (4.0–5.3) × 2.9 (2.7–3.3), NC 6–7; GBAN: MK203073. Fig. 95.	*Chelon ramada* (Risso); River Minho (Vila Nova de Cerveira), Portugal	Rocha et al. (2019b)
M. pirapitingai Capodifoglio, Adriano, Naldoni, Meira, Silva et Maia, 2020	P rounded, up to 0.2 in diameter, in pyloric caecum; SP fusiform in frontal view, 13.0 (11.7–13.8) × 4.3 (4.0–4.6) × 3.8 (3.5–4.3), with caudal processes longer than spore body, 44.7 (40.5–48.1), giving a SP total length of 57.5 (52.4– 61.6); PC elongated, equal, 6.3 (5.6–7.3) × 1.6 (1.3–2.0), NC 4; GBAN: MK492647. Fig. 96.	*Piaractus brachypomus* (Cuvier); Tapajós River, Municipality of Santarém, Pará State, Brazil	Capodifoglio et al. (2020b)
M. pronini Liu, Batueva, Zhao, Zhang, Zhang, Li et Li, 2016	A single big oval and yellowish P, 14 × 9.3 free in abdominal cavity in two hosts from Russia, and several small oval and yellowish P, 0.85 × 0.65 mm embedded in visceral serous membranes in Chinese hosts; SP elongate obovate in frontal view, lemon-shaped in sutural view, 15.1 (14.3–16.2) × 10.1 (9.6–10.8) × 6.7 (6.4–7.4) in Russian isolates, and 14.7 (13.8–15.6) × 9.6 (9.0–13.3) × 6.6 (6.2–7.2) in Chinese ones; PC pyriform, equal, 5.4 (4.3–6.7) × 3 (4.8–5.6) in Russian isolates, and 5.3 (4.8–5.6) × 3.0 (2.9–3.4) in Chinese isolates, GBAN: KU524889–KU524890 (SSU), KU524891–KU524892 (LSU) and KU524893–KU 424898 (ITS); note: the Russian locality is considered the type-locality; Chinese material is considered as from other locality. Fig. 97.	*Carassius gibelio* (Bloch); Pond near Barguzim River, Lake Baikal watershed, Russia	Liu et al. (2016b)
M. pseudowulii Zhang, Zhai, Liu et Gu, 2017	P round, black or milky white, histozoic in skin; PS pyriform in frontal view and lemon-shaped in lateral view, some spores with caudal appendages 2.2–4.5 long, 14.6 (12.9–16.2) × 9.4 (8.1–10.8) × 7.0 (6.1–8.1); PC ampullaceous, slighthly unequal in size, 7.9 (8.2–9.5) × 3.5 (3.0–3.9) the larger, and 7.4 (6.9–8.0) × 3.4 (2.9–3.9) the smaller, NC 7–9; GBAN: KY229918. Fig. 98.	*Tachysurus fulvidraco* (Richardson); fish farm in Yangchen City, Hubei, China	Zhang et al. (2017)
M. puntiusii Gupta et Kaur, 2017	P white, round to irregular, 0.8–1.0 in diameter, in caudal fin; SP ellipsoidal in frontal view and lemon-shaped and lemon-shaped in lateral view, sutural edge markings on posterior end, 7.7 ± 0.3 × 5.3 ± 0.15; PC unequal in size, the larger pyriform, 3.0 ± 0.1 × 1.8 ± 0.1, NC 6–7, the smaller pyriform or elongated, 1.7 ± 0.2 × 0.9 ± 0.1, NC 3–4; GBAN: KU516662. Fig. 99.	*Puntius sophore* (Hamilton); Ranjit Sagar Wetland, Punjab, India	Gupta and Kaur (2017b)
M. ramadus Rocha, Casal, Alves, Antunes, Rodrigues et Azevedo, 2019	P whitish and filamentous, about 2–3 in length in gill lamellae; SP spherical to subspherical in valvular view and ellipsoidal in sutural view, 8.2 (7.3–9.3) × 7.9 (7.3–8.3) × 6.4 (6.0–6.7); PC equal and pyriform, 4.2 (4.0–4.3) × 3.0 (2.7–2.3), NC 5–6; GBAN: MK203074. Fig. 100.	*Chelon ramada* (Risso); River Minho (Vila Nova de Cerveira), Portugal	Rocha et al. (2019b)
M. renalis Rocha, Casal, Alves, Antunes, Rodrigues et Azevedo, 2019	P in kidney, SP ellipsoidal to subspherical in valvular view and ellipsoidal in sutural view, 8–10 markings near sutural line, 6.7 (6.3–7.3) × 5.8 (5.3–6.0) × 4.6 (4.3–5.0); PC equal, pyriform, 3.1 (2.7–3.7) × 1.9 (2.3–3.0), NC 4; GBAN: MK203077. Fig. 101.	*Chelon ramada* (Risso); River Minho (Vila Nova de Cerveira), Portugal	Rocha et al. (2019b)
M. ridibundae Abdel-Ghaffar, Abdel-Gaber, Maher, El Deeb, Kamel, Al Quraishy et Mehlhorn, 2017	P in testicular tissue, looking tumour-like masses, often up to 20 in diameter, whitish, ovoid or ellipsoidal, 0.3 (0.1– 0.5) in diameter; SP oval in frontal view, biconvex in sutural view, rounded in anterior and posterior ends, 2 parietal folds on posterior-lateral margins of shell valves, 9.6 (8.9 –11.5) × 8.4 (7.5–9.1); PC pyriform, equal, 5.2 (4.3–5.9) × 3.1 (2.2–3.6), NC 5–6. Fig. 102.	*Pelophylax ridibundus* (Pallas); Kafr El-Sheikh Governorate, Egypt	Abdel-Ghaffar et al. (2017)
M. saladensis Marcotegui et Martoreli, 2017	P in gill filaments and gill rakers; SP pyriform, rounded in valvular view and biconvex in sutural view, valves smooth, 10.6 (10.0–11.1) × 9.2 (8.4–9.7) × 4.1 (2.6–4.9); PC equal, pyriform, 3.8 (3.3–4.0) × 2.3 (2.1–2.4), NC 4–5. Fig. 103.	*Mugil liza* Valenciennes; Salado River, Samborombón, Buenos Aires, Argentina	Marcotegui and Martorelli (2017)
M. sanagaensis Folefack, Defoueng et Fomena, 2017	P white, ovoid or subspherical in heart auricles, 0.14–0.27 × 0.65–0.195; SP ovoid with both rounded ends, 9.9 (9.4–11) × 6.8 (6.1–7.3), valves with 5–6 folds at posterior end; PC pyriform, slightly unequal in size, 4.6 (4.1–5.1) × 4 (3.2–4.3), NC 8–10 the larger, 2.3 (2–2.6) × 2.1 (1.8–2.3), NC 6–7 the smaller. Fig. 104.	*Enteromius callipterus* (Boulenger); Lébamzip, Sanaga River, Cameroon	Folefack et al. (2017)
M. sessabai Folefack, Defoueng et Fomena, 2017	P whitish and spherical under skin and in kidney, 0.350 × 0.345; SP ovoid with rounded ends, 6–7 valvular folds at posterior end, 13.4 (12.6–14) × 10.8 (9.9–11.5); PC equal, pyriform, 5.9 (5–6) × 3.4 (2.5–3.8), NC 8–10; well-developed IP, 2.6 (2.1–3.2). Fig. 105.	*Enteromius callipterus* (Boulenger) Lébamzip, Sanaga River, Cameroon	Folefack et al. (2017)
M. sheyangensis Liu, Yuan, Zhao, Fang, Chen et Zhang, 2016	P rounded or ellipsoid in gill filaments, usually in middle part of filaments; SP flat-pear shaped in frontal view and elongated-shaped in sutural view, smooth, some spores with typical *Henneguya*-like caudal appendage, 11.0 (10.5–11.9) × 10.2 (9.2–10.7) × 6.3 (5.9–6.9); PC pyriform, equal, 5.5 (4.5–6.1) × 3.4 (2.9–4.0), NC 7–8; distinct IP present; GBAN: KU313484 and KU313485. Fig. 106.	*Carassius gibelio* (Bloch); Shenyang County, Yancheng City, East China	Liu et al. (2016c)
M. sonarpurensis Ghosh et Bandyopadhyay, 2017	P rounded, 2–3 in diameter, attached to mucous membrane of gill lamellae; SP water droplet shaped in valvular view, surface smooth, 12.1 (11.0–13.2) × 6.7 (5.9–6.1); PC slender and elongate, unequal in shape, 8.8 × 3.0 and 7.7 × 3.1. Fig. 107.	*Labeo bata* (Hamilton); Sonarpur, West Bengal, India	Ghosh and Bandyopadhyay (2017)

M. stellatus Stilwell, Petty, Camus, Woodyard, Griffin et Rosser, 2020	P disseminated throughout cranial nerves and ganglia of head and body wall, forming space occupying masses approximately 80-100 µ in diameter; SP pyriform, rounded posteriorly and tapering anteriorly, 18.4 (17.0–19.4) × 8.8 (8.2–9.3) × 7.2 (6.7–7.5); PC pyriform, with neck-like projection at apical end, unequal, the larger 9.9 (9.1–10.7) × 5.4 (4.9–6.3), NC 8–10, the smaller 5.0 (4.3–5.9) × 2.6 (2.2–3.1), NC 4– 6; IP absent; GBAN: NM795057. Fig. 108.	*Thoracocharax stellatus* (Kner); Colombia (wild caught, imported for pet trade)	Stilwell et al. (2020b)
M. szentendrensis Cech, Borzák, Molnár et Székely, 2015	P small, round to roundish, 0.06–0.13 in diameter, in capillary network of gill lamellae; SP pyriform in frontal view, with well-defined extrusion at anterior end, 9.2 (8.8–9.6) × 7.9 (7.6–8.0) × 6.7 (6.4–7.1): PC pyriform, equal, 5.3 (4.8–5.6) × 3.0 (2.8–3.2), NC 6; IP absent; GBAN: KP025684–KPO25686. Fig. 109.	*Chondrostoma nasus* (Linnaeus); River Danube at Szentendre, Hungary	Cech et al. (2015)
M. taibaiensis Liu, Hua, Zhang, Zhao, Zhang et Zhang, 2017	P ellipsoidal, 1.7–2.9 × 0.9–1.7 in circular muscle layer of inner intestinal wall; SP ellipsoidal in frontal view and lemon-shaped in lateral and apical view, valves smooth, 10.8 (10.2–11.2) × 9.6 (9.1–9.9) × 6.3 (6.1–6.6); PC equal, pyriform, 5.0 (4.4–5.4) × 3.4 (3.2–3.6), NC 4–5; GBAN: KU928249. Fig. 110.	*Cyprinus carpio* Linnaeus; Huangmei County, Hubei Province, China	Liu et al. (2017)
M. tanakai Kato, Kasai, Tomochi, Li et Sato, 2017	P ellipsoidal, 0.55 (0.37–0.82) × 0.42 (0.26–0.63), or 0.32 (0.20–0.39) × 0.25 (0.15–0.34) in intralamellar tissue adjacent to vessels in gill filaments; SP elongated, pyriform in valvular and sutural views, 17.2 (15.4–16.8) × 6.8 (6.3–8.4) × 6.3 (5.9–6.8); PC pyriform, equal in size (sometimes unequal), 8.7 (7.6–9.4) × 2.4 (2.0–2.7), NC 8–10; GBAN: LC 228235 and LC 228236. Fig. 111.	*Cyprinus carpio* Linnaeus; Kurokawa (Fushinogawa River), Yamaguchi City, Japan	Kato et al. (2017)
M. tapajosi Zatti, Atkinson, Maia, Corrêa, Bartholomew et Adriano, 2018	P whitish, oval and polysporic, up to 5 in diameter, in base of gill filaments; SP smooth, with equal valves, round to oval in frontal view, biconvex in lateral view, 15 (13.5–17) × 10.7 (9.6–11.4); PC elongated, equal, 5 (4.6–7.1) × 3 (2.3–3.8), NC 6–7; GBAN: MF193890. Fig. 112.	*Brachyplatystoma rousseauxii* (Castelnau); Tapajós River, Santarém, Pará State, Brazil	Zatti et al. (2018)
M. tchoumbouei Fonkwa, Tchuinkam, Tomedi et Tchoumboue, 2017	P whitish, ovoid, 1–2 in diameter, in fins, skin and operculum; SP pear-shaped with rounded ends and sometimes flattened anterior end, 19.1 (17.5–25.5) × 8.8 (7.5–10); PC inequal in size, 7.6 (6–8.7) × 3 (2.5–3.7) the larger, 7.0 (5.6–8.7) × 2.6 (1.8–4.5) the smaller, NC 7–10. Fig. 113.	*Enteromius callipterus* (Boulanger); Mapé River, Bankim, Adamawa, Cameroon	Fonkwa et al. (2017)
M. upmae Gupta et Kaur, 2020	In gills (intralamellar vascular type), P cylindrical to round, white, 0.4–1.5 in diameter; SP pyriform with elongated anterior end and rounded posterior one, valves symmetrical, 9.6 × 5.0; PC subequal and pyriform, the larger 4.3 × 2.3, the smaller 4.0 × 2.1, NC 10–11 and 8–9 in the larger and smaller, respectively; IP absent; GBAN: KX757026. Fig. 114.	*Hypophthalmichthys nobilis* (Richardson), Ranjit Sagar Wetland, Punjab, India	Gupta and Kaur (2020)
M. urinaris Rocha, Casal, Alves, Antunes, Rodrigues et Azevedo, 2019	P in urinary bladder; SP ellipsoidal in valvular view, 10.0 (9.3–10.3) × 8.2 (7.7–8.7); PC equal, pyriform, 4.0 (3.3–3.7) × 2.8 (2.7–3.0); NC 4–5; GBAN: MK203083. Fig. 115.	*Mugil cephalus* Linnaeus; River Minho (Vila Nova de Cerveira), Portugal	Rocha et al. (2019b)
M. vascularis Ahmad et Kaur, 2017	P in gills, rounded, 0.05 in diameter, or highly elongated, 3.0 × 0.7; SP pyriform, with sharply pointed anterior end and rounded posterior one, 10.7 (9.7–11.7) × 4.8 (3.8–5.8); PC equal, elongate, pyriform, 6.5 (5.4–7.5<) × 1.8 (1.1–2.5), NC 8–9; IP absent. Fig. 116.	*Cirrhinus mrigala* (Hamilton, 1822), nursery ponds in Village Fagan majra, District Fatehgarh Sahib, Punjab, India	Ahmad and Kaur (2017)
M. vesicularis Rocha, Casal, Alves, Antunes, Rodrigues et Azevedo, 2019	P in gall bladder wall; SP ellipsoidal in valvular and sutural view, with smooth surface, 10–15 markings near suture line, 11.9 (11.3–12.7) × 10.3 (10.0–10.7) × 6.5 (6.0–6.7); PC pyriform, equal, 4.9 (4.7–5.3) × 3.1 (2.7–3.7), NC 4–5; GBAN: MK203085. Fig. 117.	*Mugil cephalus* Linnaeus; River Minho (Vila Nova de Cerveira), Portugal	Rocha et al. (2019b)
M. vetuschicanus Naldoni, Carriero, Moreira, Silva, Maia et Adriano, 2020	P in fins, white and spherical, 0.15–0.5; SP round in frontal view, and biconvex in lateral view, 10 (10.7–11.5) × (8.1–8.8) in frontal view x 5.4 (5.3–5.5) in thickness in lateral view; PC equal, elongated, 4.7 (4.4–5.3) × 2.3 (1.5–2.7), NC 8, GBAN: MT302613. Fig. 118.	*Salminus franciscanus* Flávio, Lima et Britsky; São Francisco River, Pirapora, Minas Gerais State, Brazil	Naldoni et al. (2020a)
M. xiantaoensis Tahir, Guo, Zhao, Liu et Gu, 2019	P forming pinkish flower-like aggregates on surface of fins hemisegments, mostly at tips of fins; SP pyriform in frontal view, biconvex in sutural view, pointed anteriorly and rounded posteriorly, 12.6 (11.3–13.9) × 9.9 (8.4–11.1) × 7.1 (6.1–7.7); PC unequal and eggplant-shaped, the larger 6.8 (6.0–8.1) × 3.4 (3.0–3.8), the smaller 6.4 (5.5–7.4) × 3.6 (3.2–3.9), NC 6–8 in both; IP almost 1/6th of the SP total length; GBAN: KY421105. Fig. 119.	*Tachysurus fulvidraco* (Richardson); Fish farm in Xiantao, Hubei, China	Tahir et al. (2019)
M. xinyangensis Wu, Wang, Sato et Zhang, 2019	P round and yellowish, about 4–5 in diameter, located bilaterally, dorsal to two opercular openings, with 2 and 3 connected plasmodia in left and right side of operculum; SP orbicular in frontal view, 9.4 (8.7–10.6) × 8.6 (7.3–9.5) × 6.4 (5.8–7.1); PC pyriform, slightly unequal, 5.6 (4.3–6.8) × 3.0 (2.4–3.6), NC 4–5; GBAN: AF001579. Fig. 120.	*Abbottina rivularis* (Basilewsky); Huang River, Xinyang City, Henan, China	Wu et al. (2019)
M. zoohuri Majunder, Panda, Ghosh et Bandyopadhyay, 2015	P in gills lamellae, creamy white, rounded, 2–3 in diameter; SP tear-shaped, anterior end triangular and posterior one blunt semicircular, 14.8 (13.2–17.3) × 6.3 (4.9–7.0); PC unequal, the larger 11.1 (10.4–12.0) × 2.8 (2.2–3.1), NC 17–18, the smaller 10.6 (10.1–11.2) × 2.7 (2.0–3.0), NC 15–16. Fig. 121.	*Cirrhinus mrigala* (Hamilton); Canning, South 24 Parganas, West Bengal, India	Majumder et al. (2015)

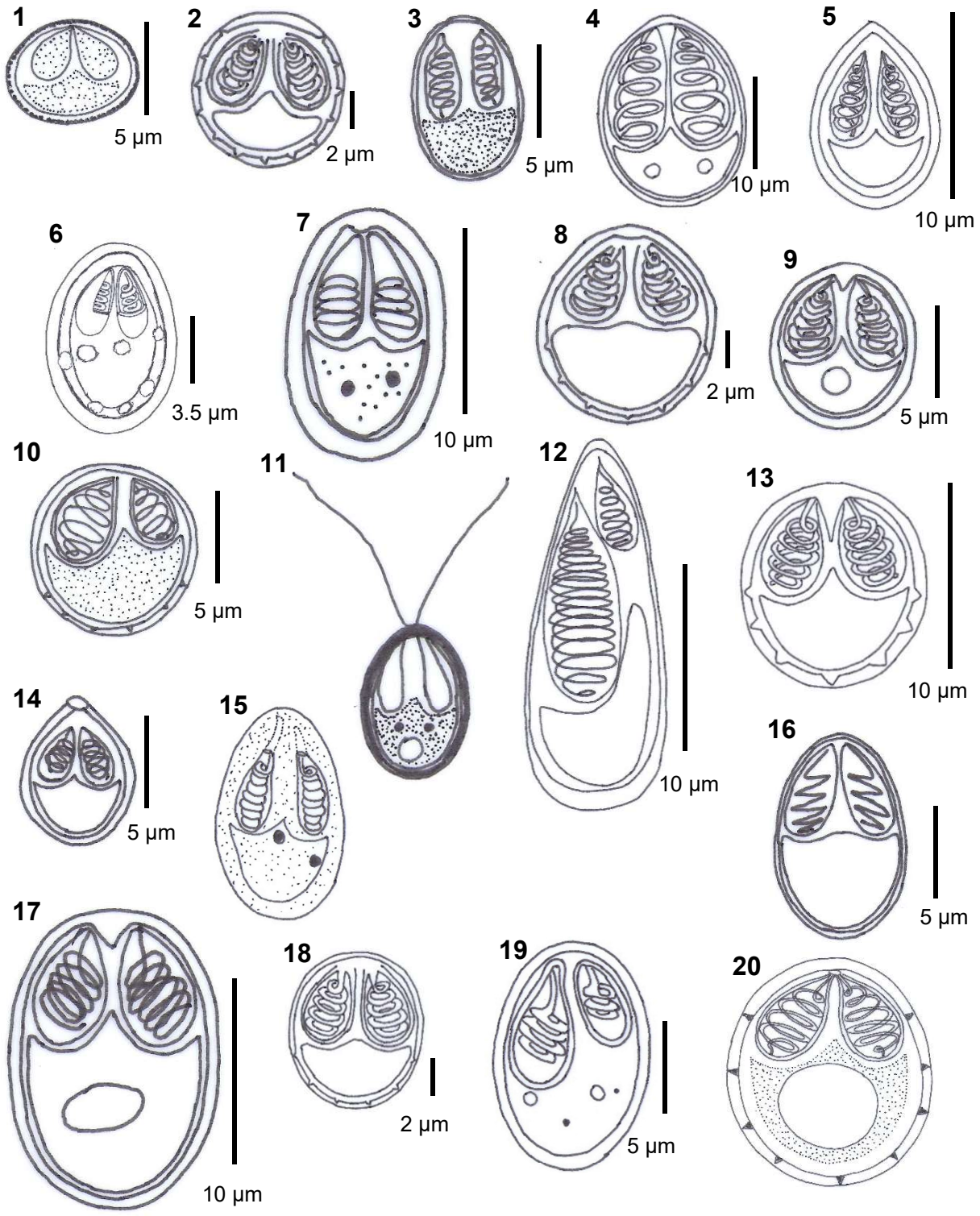

Fig. 1–20. Diagrammatic illustrations of spores of species of *Myxobolus* Bütschli, 1882. **1** – *M. adeli*; **2** – *M. adiposus*; **3** – *M. adlardi*; **4** – *M. adrianoi*; **5** – *M. anatolicus*; **6** – *M. arariensis*; **7** – *M. arapiunsus*; **8** – *M. arcasii*; **9** – *M. arrabonensis*; **10** – *M. atkinsoni*; **11** – *M. awadhii* (not to scale); **12** – *M. axelrodi*; **13** – *M. balatonicus*; **14** – *M. basuhaldari*; **15** – *M. batalhensis* (not to scale); **16** – *M. bejeranoi*; **17** – *M. bjoerknae*; **18** – *M. cerveirensis*; **19** – *M. chanosi*; **20** – *M. chushi* (not to scale). Redrawn from the original descriptions (see Table 1 for references).

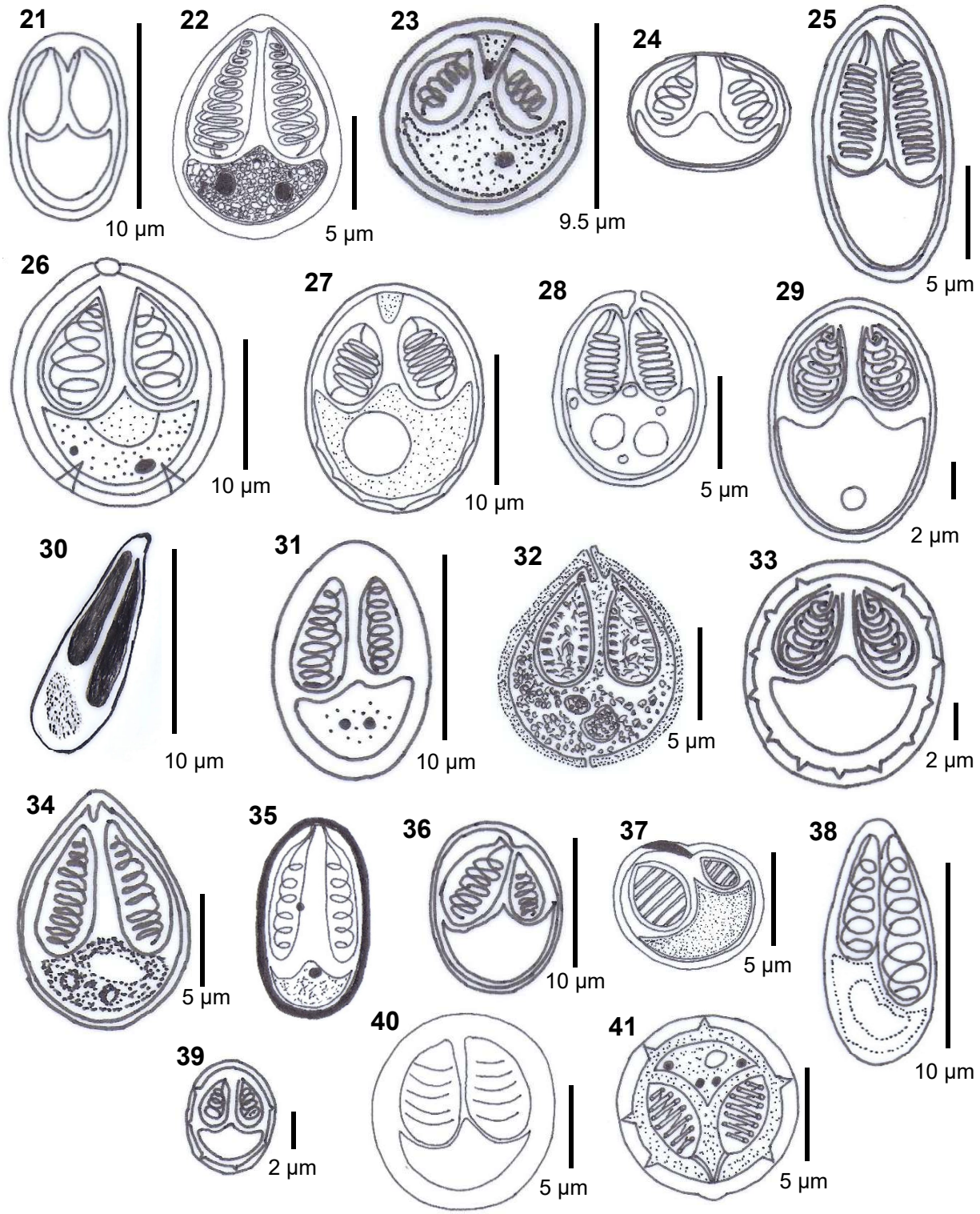

Figs. 21–41. Diagrammatic illustrations of spores of species of *Myxobolus* Bütschli, 1882. **21** – *M. cultrati*; **22** – *M. curimatae*; **23** – *M. danrici*; **24** – *M. deformis* (not to scale); **25** – *M. dermatoulcerans*; **26** – *M. dermiscalis*; **27** – *M. dibombensis*; **28** – *M. doubleae*; **29** – *M. duriensis*; **30** – *M. elongatum*; **31** – *M. figueirae*; **32** – *M. filamentum*; **33** – *M. galaicoportucalensis*; **34** – *M. ginbuna*; **35** – *M. gomtii* (not to scale); **36** – *M. gutturocola*; **37** – *M. hardevi*; **38** – *M. harpreetae*; **39** – *M. hepatobiliaris*; **40** – *M. hilarii*; **41** – *M. himalayaensis*. Redrawn from the original descriptions (see Table 1 for references).

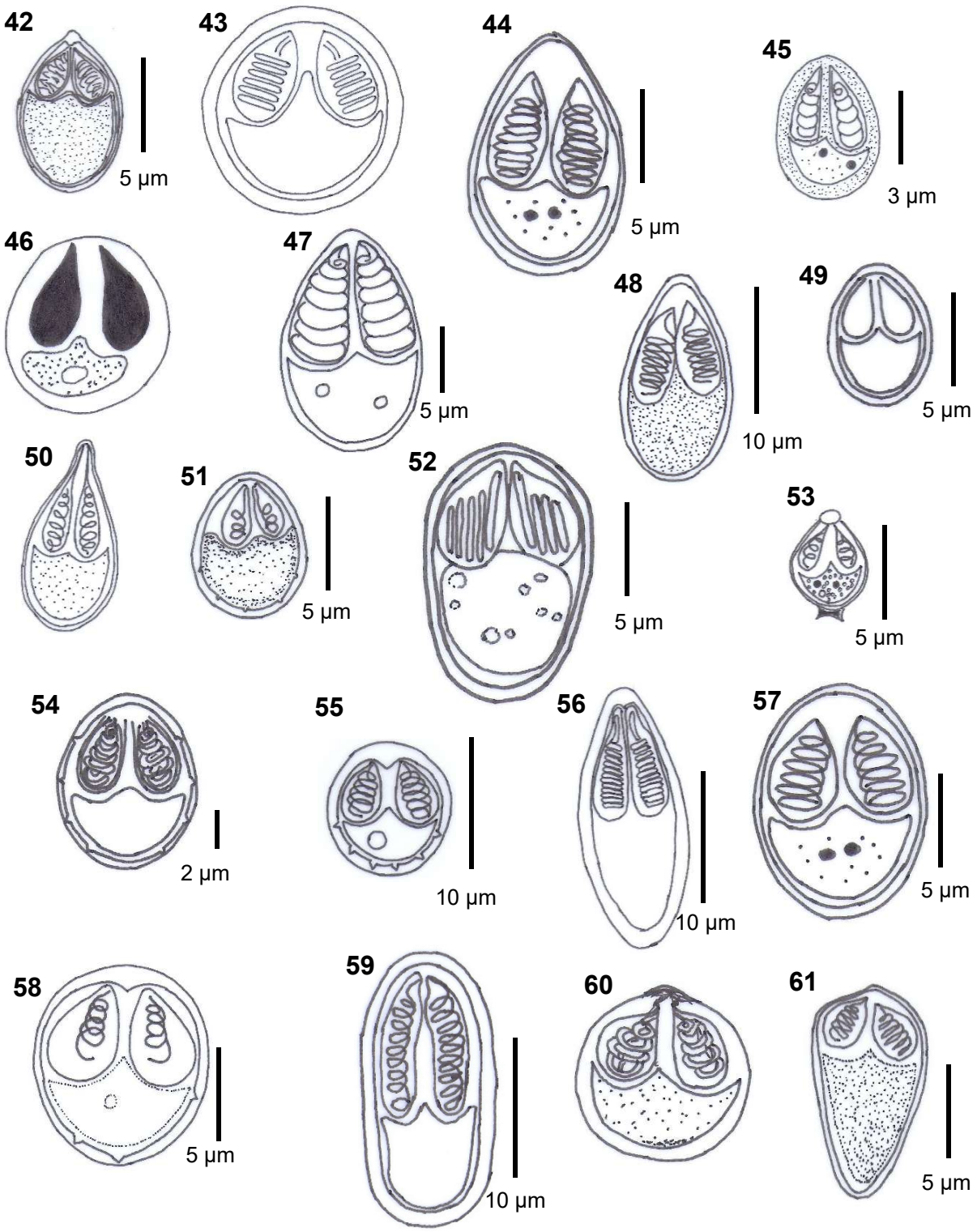

Figs. 42–61. Diagrammatic illustrations of spores of species of *Myxobolus* Bütschli, 1882. **42** – *M. holzerae*; **43** – *M. ictiobus* (not to scale); **44** – *M. iecoris*; **45** – *M. imparfinis*; **46** – *M. indica* (not to scale); **47** – *M. iquitoensis*; **48** – *M. jialingensis*; **49** – *M. kalavatiae*; **50** – *M. kashmirensis* (not to scale); **51** – *M. khaliji*; **52** – *M. klamathellus*; **53** – *M. knobii*; **54** – *M. labrosus*; **55** – *M. lamellobasis*; **56** – *M. lepomis*; **57** – *M. lienis*; **58** – *M. linzhiensis*; **59** – *M. longissimus*; **60** – *M. lucknowii* (not to scale); **61** – *M. magai*. Redrawn from the original descriptions (see Table 1 for references).

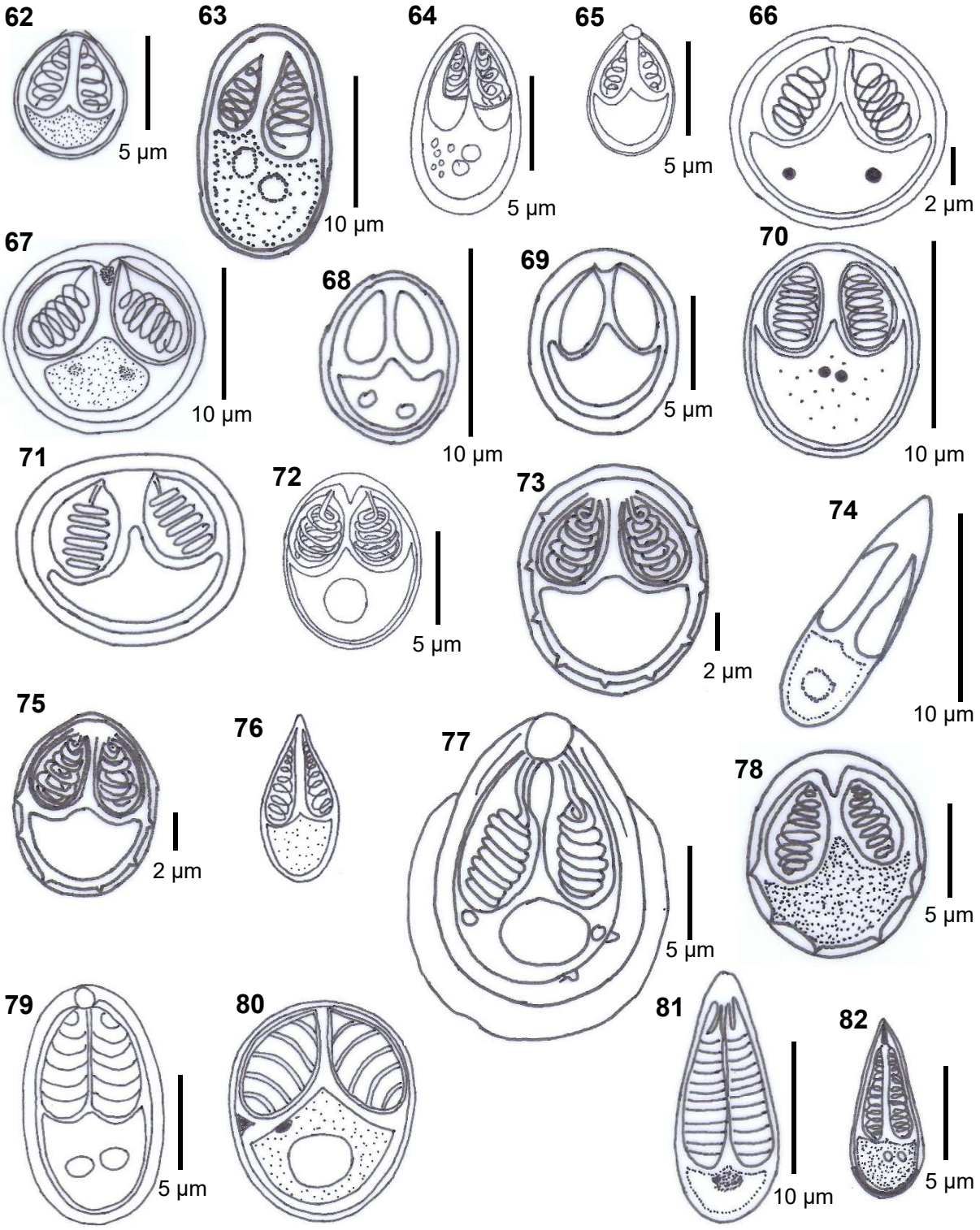

Figs. 62–82. Diagrammatic illustrations of spores of species of *Myxobolus* Bütschli, 1882. **62** – *M. majraiensis*; **63** – *M. mapei*; **64** – *M. marajoensis*; **65** – *M. markiwi*; **66** – *M. mauriensis*; **67** – *M. marumotoi*; **68** – *M. matosi*; **69** – *M. meerutensis*; **70** – *M. mineirus*; **71** – *M. minutus* (not to scale); **72** – *M. mucosus*; **73** – *M. mugiliensis*; **74** – *M. muralidharani*; **75** – *M. muscularis*; **76** – *M. nanokiensis* (not to scale); **77** – *M. neurofontinalis*; **78** – *M. ngassmi*; **79** – *M. niger*; **80** – *M. nigerai* (not to scale); **81** – *M. nilimae*; **82** – *M. okamurae*. Redrawn from the original descriptions (see Table 1 for references).

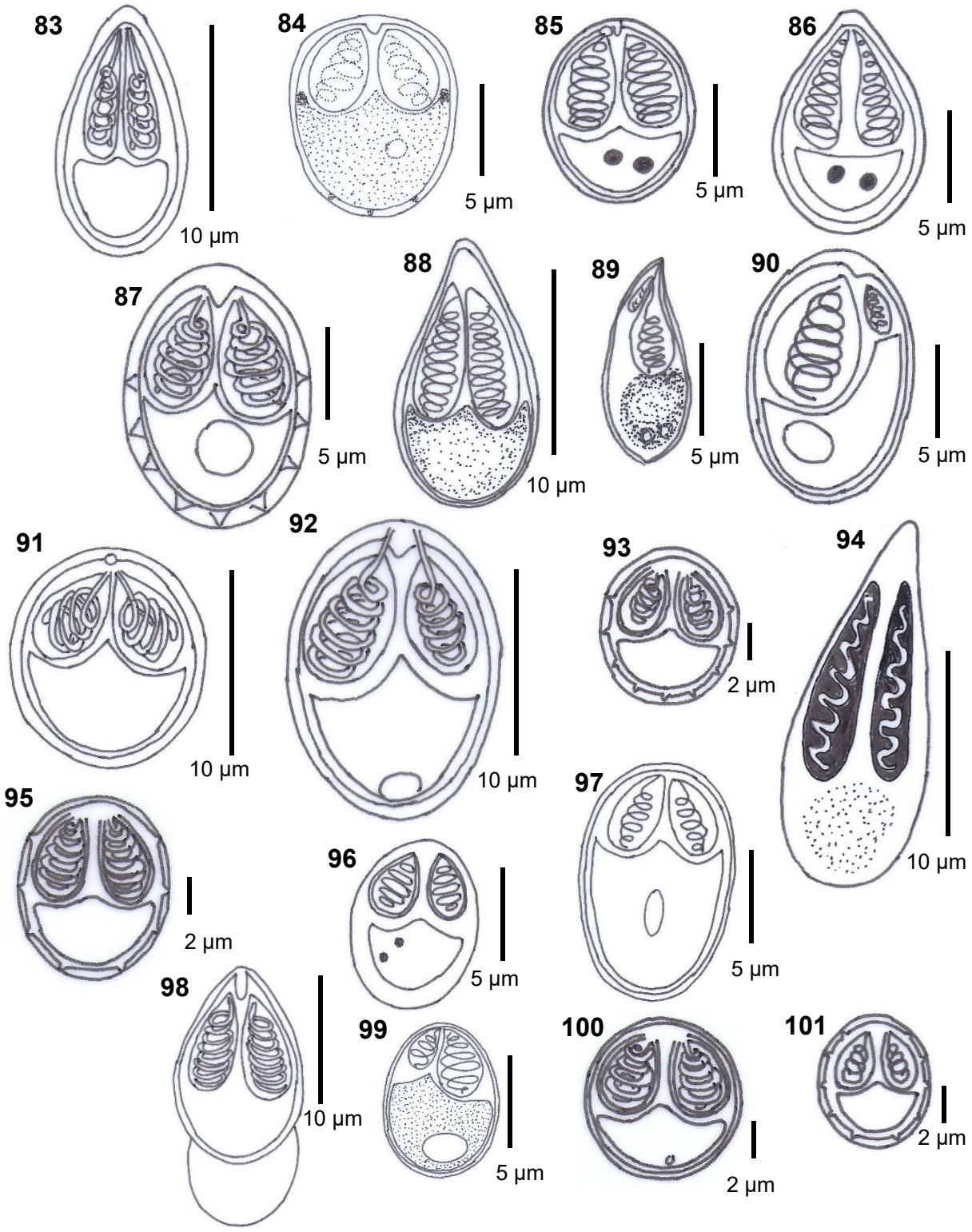

Figs. 83–101. Diagrammatic illustrations of spores of species of *Myxobolus* Bütschli, 1882. **83** – *M. ompok*; **84** – *M. oralis*; **85** – *M. orthotaenae*; **86** – *M. ovarium*; **87** – *M. paksensis*; **88** – *M. parakoi*; **89** – *M. paratoyamai*; **90** – *M. paratypicus*; **91** – *M. peleci*; **92** – *M. pelecicola*; **93** – *M. peritonaeum*; **94** – *M. petalum*; **95** – *M. pharyngobranchialis*; **96** – *M. pirapitingae*; **97** – *M. pronini*; **98** – *M. pseudowulii*; **99** – *M. puntiusii*; **100** – *M. ramadus*; **101** – *M. renalis*. Redrawn from the original descriptions (see Table 1 for references).

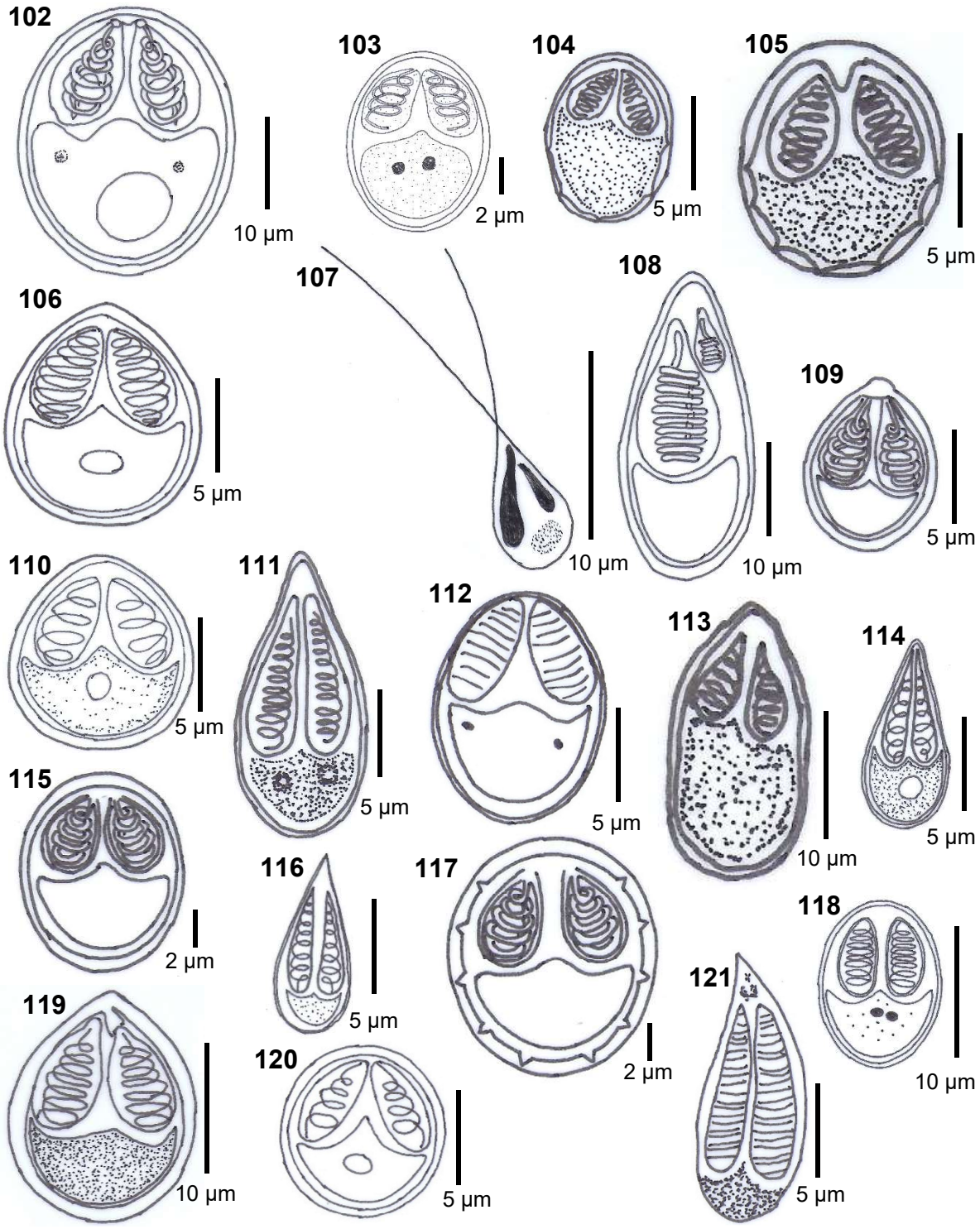

Figs. 102–121. Diagrammatic illustrations of spores of species of *Myxobolus* Bütschli, 1882. **102** – *M. ridibundae*; **103** – *M. saladensis*; **104** – *M. sanangaensis*; **105** – *M. sessabai*; **106** – *M. sheyangensis*; **107** – *M. sonarpurensis*; **108** – *M. stellatus*; **109** – *M. szentendrensis*; **110** – *M. taibaiensis*; **111** – *M. tanakai*; **112** – *M. tapajosi*; **113** – *M. tchoumbouei*; **114** – *M. upmae*; **115** – *M. urinaris*; **116** – *M. vascularis*; **117** – *M. vesicularis*; **118** – *M. vetuschicanus*; **119** – *M. xiantaoensis*; **120** – *M. xinyangensis*; **121** – *M. zoohuri.* Redrawn from the original descriptions (see Table 1 for references).

REFERENCES

Abdel-Ghaffar F., Abdel-Gaber R., Maher S., El Deeb N., Kamel R., Al Quraishy S., Mehlhorn H. 2017: Morphological and ultrastructural characteristics of *Myxobolus ridibundae* n. sp. (Myxosporea: Bivalvulida) infecting the testicular tissue of the marsh frog *Rana ridibunda* (Amphibia: Ranidae) in Egypt. Parasitol. Res. 116: 133–141.

Abidi R., Fariya N., Chahan U.K. 2016: Morphological description of *Myxobolus gomtii* sp. nov. infecting *Labeo rohita* (Hamilton, 1882) from river Gomti at Lucknow in Uttar Pradesh. J. Appl. Biosci. 42: 36–41.

Abidi R., Fariya N., Irshan M., Chauhan U.K. 2015: A new species of myxozoan parasite, *Myxobolus lucknowii* sp. nov., in kidney of *Clarias batrachus* Linn. from river Gomti at Lucknow. Trends Parasitol. Res. 4: 5–11.

Abrunhosa J., Sindeaux-Neto J.L., Santos A.K., Hamoy I., Matos E. 2018a: A new species of Myxozoa in the skeletal striated musculature of *Rhamdia quelen* (Quoy and Gaimard) (Siluriforme: Pimelodidae) Amazonian fish, Marajá Island, Brazil. Zootaxa 4482: 164–176.

Abrunhosa J., Sindeaux-Neto J.L., Santos A.K., Hamoy I., Matos E. 2018b: *Myxobolus marajoensis* sp. n. (Myxosporea: Myxobolidae), parasita do bagre de água doce *Rhamdia quelen* da região da Amazônia brasileira. Braz. J. Vet. Parasitol. 26: 465–471.

Ahmad I., Kaur H. 2017: *Myxobolus vascularis* n. sp. (Cnidaria: Myxozoa: Myxosporea), a new parasite infecting fingerlings of Indian major carps in aquaculture in Punjab, India. Bull. Pure Appl. Sci. 2: 57–70.

Ahmed I., Ahmad I., Dar S.A., Awas M., Kaur H., Ganai B.A., Shah B.A. 2019: *Myxobolus himalayaensis* sp. nov. (Cnidaria: Myxozoa) parasiting *Schizothorax richardsonii* (Cyprinidae: Schizothoracinae) from River Poonchin, North West Himalaya, India. Aquacul. Reports 14: 100192.

Atkinson S.D., Banner C.R. 2017: A novel myxosporean parasite *Myxobolus klamathellus* n. sp. (Cnidaria, Myxosporea) from native blue chub (*Gila coerulea*) in Klamath Lake, Oregon. Parasitol. Res. 116: 299–302.

Borzák R., Molnár K., Cech G., Papp M., Déak-Paulus P., Székely C. 2016: Description of two new species of *Myxobolus* Bütschli, 1892, *M. peleci* n. sp. and *M. cultrati* n. sp., detected during an intensive mortality of the sichel, *Pelecus cultratus* (L.) (Cyprinidae), in Lake Balaton, Hungary. Syst. Parasitol. 93: 667–677.

Camus A.C., Dill J.A., Rosser T.G., Pote L.M., Griffin M.J. 2017: *Myxobolus axelrodi* n. sp. (Myxosporea: Myxobolidae) a parasite infecting the brain and retinas of the cardinal tetra *Paracheirodon axelrodi* (Teleostei: Characidae). Parasitol. Res. 116: 387–397.

Camus A.C., Griffin M. 2010: Molecular Characterization and Histopathology of *Myxobolus koi* infecting the Gills of a Koi, *Cyprinus carpio*, with an Amended Morphological Description of the Agent. J. Parasitol. 96(1): 116-124.

Capodifoglio K.R.H., Meira C.M., Silva M.R.M., Corrêa L.L., Adriano E.A., Maia A.A.M. 2020a: Morphology and molecular data of two novel cnidarian myxosporean (Myxobolidae) infecting *Piaractus brachypomus* from the Amazon basin. Acta Trop. 209: 105533.

Capodifoglio K.R.H., Adriano A.E., Naldoni J., Meira C.M., Silva M.R.M., Maia A.A.M. 2020b: Novel myxosporean species parasitizing an economically important fish from the Amazon basin. Parasitol. Res. 119: 1209–1220.

Capodifoglio K.R.H., Adriano E.A., Silva M.R.M., Maia A.A.M. 2019: The resolution of the taxonomic dilemma of *Myxobolus colossomatis* and description of two novel myxosporeans species of *Colossoma macropomum* from Amazon basin. Acta Trop. 191: 17–23.

Capodifoglio K.R.H., Adriano E.A., Milanin T., Silva M.R.M., Maia A.A.M. 2015: Morphological, ultrastructural and phylogenetic analyses of *Myxobolus hilarii* n. sp. (Myxozoa, Myxosporea), a renal parasite of farmed *Brycon hilarii* in Brazil. Parasitol. Int. 65: 184–190.

Cardim J., Silva D., Hamoy I., Matos E., Abrunhosa F. 2018: *Myxobolus bragantinus* n. sp. (Cnidaria: Myxosporea) from the gill filaments of the redeye mullet, *Mugil rubrioculus* (Mugiliformes: Mugilidae), on the eastern Amazon coast. Zootaxa 4482: 177–187.

Cech G., Borzák R., Molnár K., Székely C. 2015: Three new species of *Myxobolus* Bütschli, 1882 (Myxozoa: Myxobolidae) infecting the common nase *Chondrostoma nasus* (L.) in the River Danube. Syst. Parasitol. 92: 101–111.

Chandran A., Zacharia P.U., Sanil N.K. 2019: *Myxobolus chanosi* n. sp., a novel myxosporean infecting *Chanos chanos* (Forsskåll, 1775) from Allapuzha, along the Soutwest coast of India. J. Coastal Res. 86 (Suppl.): 128.

Chaudhary A., Goswami U., Gupta A., Cech G., Singh H.S., Molnár K., Székely C., Shama B. 2018: Morphological, histological and molecular description of *Myxobolus ompok* n. sp. (Myxosporea: Myxobolidae), a kidney myxozoan from Pabdah catfish *Ompok pabda* (Hamilton, 1822) (Silurigormes: Siluridae) in India. Parasitol. Res. 117: 1899–1905.

Dar S.A., Kaur H., Chishti M.Z. 2017a: *Myxobolus chushi* n. sp. (Myxozoa: Myxosporea) parasitizing *Schizothorax niger* (Heckel), a native cyprinid fish from Wullar Lake in Kashmir Himalayas. Parasitol. Int. 66: 272–278.

Dar S.A., Kaur H., Chishti M.Z. 2017b: First record of myxozoan parasites from fresh water fishes of Jammu and Kashmir and their pathogenicity. Microbial. Pathog. 105: 138–144.

Deli A., Lekeufack F.G.B., Fomena A. 2017: Description of *Myxidium tetraodoni*, sp. nov, *Myxidium anisocapsularis*, sp. nov. and *Myxobolus magai* sp. nov. (Myxosporea: Bivalvulida) infecting some freshwater fishes in Cameroon (Central Africa). Fisheries Aquac. J. 8: 235.

Dar S.A., Kaur H., Chishti M.Z. 2016: Morphological and histopathological description of *Myxobolus nigerae* n. sp. infecting gills of a cold water native cyprinid fish, *Schizothorax niger*, from Wullar Lake (India). Species 17: 109–118.

Eiras J.C., Zhang J., Molnár K. 2014: Synopsis of the species of *Myxobolus* Bütschli, 1882 (Myxozoa, Myxosporea, Myxobolidae) described between 2005 and 2013. Syst. Parasitol. 81: 11–36.

Eiras J.C., Molnár K., Lu Y.S. 2005: Synopsis of the species of the genus *Myxobolus* Bütschli, 1882 (Myxozoa, Myxosporea, Myxobolidae). Syst. Parasitol. 61: 1–46.

Fariya N., Abidi R., Chauhan U.K. 2018a: Description of new myxozoan parasite *Myxobolus awadhii* sp. nov from the gills of freshwater catfish *Clarias batrachus* Linn. J. Parasitic Dis. 42: 598–603.

Fariya N., Abidi R., Chauhan U.K. 2018b: *Myxobolus deformis* sp. nov. (Myxozoa, Myxosporea, Myxobolidae), a new myxosporean parasite infesting the gills of *Cyprinus carpio*. Species 19: 4–14.

Folefack G.B.L., Abdel-Baki A.S., Ateba N.O.O., Fomena A., Mansour L. 2019: Morphological and molecular characterization of *Myxobolus dibombensis* sp. n. (Myxozoa: Myxobolidae), a parasite of the African carp *Labeobarbus batesii* (Teleostei: Cyprinidae) from Dibombe River, Cameroon. Parasitol. Res. 118: 763–771.

Folefack G.B.L., Defoueng N.A.S., Fomena A. 2017: Three new species of *Myxobolus* (Myxosporea: Myxobolidae), parasites of *Barbus callipterus* Boulenger, 1907 in Cameroon. Asian J. Biol. Sci. 10: 110–120.

Froese R., Pauly D. (Eds.) 2019: FishBase. World Wide Web electronic publication. www.fishbase.org (12/2019).

Gao L., Zhang J., Yang C., Zhao Y. 2020: *Myxobolus jialingensis* n. sp. (Myxozoa: Myxobolidae) infecting urinary bladder and hepatopancreas of yellow catfish *Tachysurus fulvidraco* from China. Zootaxa 4819: 179–186.

Georges F., Timoléon T., Minette T.E., Joseph T. 2017: Two new species of *Myxobolus* (Myxozoa: Myxosporea) parasites of *Barbus callipterus* Boulenger, 1907 (Cyprinidae) and *Oreochromis niloticus* Linnaeus, 1758 (Cichlidae) in Cameroon. J. Res. Biol. 7(7): 2355–2360.

Ghosh S., Bandyopadhyay P.K. 2017: Description of three new species of the genus *Myxobolus* infecting carp fishes of India. J. Parasitic Dis. 41: 155–166.

Ghosh S., Bandyopadhyay P.K. 2016: Morphotaxonomical description of three new species of *Myxobolus* Bütschli, 1882 (Myxozoa: Myxosporea: Bivalvulida) from edible freshwater fishes of West Bengal, India. J. Parasitic Dis. 41: 97–105.

Gupta A., Kaur H. 2020: Two new species of *Myxobolus* (Cnidaria: Myxosporea) infecting freshwater fishes of Ranjit Sangar Wetland, Punjab, India. Microbial. Pathog. 147: 104421.

Gupta A., Kaur H. 2018a: 18S and 28S rDNA identity and phylogeny of two novel myxosporeans infecting gills of cyprinid carps inhabiting a coldwater wetland in northern India. Microbial. Pathog. 120: 97–108.

Gupta A., Kaur H. 2018b. *Myxobolus okamurae* sp. nov. (Myxosporea: Myxozoa) causing severe gill myxoboliosis in the cyprinid *Labeo bata* in a cold water wetland, Punjab (India). Microbial. Pathog. 115: 86–92.

Gupta A., Kaur H. 2017a: A new pathogen, *Myxobolus holzerae* (Myxosporea: Myxozoa) causing severe gill disease in an Indian major carp *Labeo rohita* in a cold-water wetland, Punjab (India). Microbial. Pathog. 111: 244–251.

Gupta A., Kaur H. 2017b: Morphological and molecular characterization of *Myxobolus puntiusii* n. sp. (Cnidaria: Myxosporea) infecting *Puntius sophore* Hamilton, 1822 from Ranjit Sagar Wetland, Punjab (India). Turk. J. Zool. 41: 1–9.

Gupta A., Kaur H. 2016: Morphological and histopathological description of *Myxobolus adlardi* n. sp. (Cnidaria: Myxosporea: Myxozoa) infecting an Indian major carp, *Labeo rohita* Hamilton, 1822 from a cold-water wetland in Punjab (India). Bull. Pure Appl. Sci. 35: 39–52.

Kato E., Kasai A., Tomochi H., Li Y.C., Sato H. 2017: Four *Myxobolus* spp. (Myxosporea: Bivalvulida) from the gill lamellae of common carp (*Cyprinus carpio*) and Japanese silver crucian carp (*Carassius langsdorfii*) in the western part of Japan, with the description of three new species (*M. tanakai* n. sp., *M. paratoyamai* n. sp., and *M. ginbuna* n. sp.). Parasitol. Res. 116: 2427–2441.

Kaur H., Ahmad I. 2017: A report on two new myxozoan parasites infecting gills of fingerlings of Indian major carps cultured in nursery ponds in Punjab (India). J. Parasitic Dis. 41: 987–996.

Kaur H., Ahmad I. 2016: Morphological description of *Myxobolus markiwi* n. sp. (Cnidaria: Myxosporea: Myxozoa) infecting gills of fingerlings of aquaculture ponds from Punjab, India. Species 17: 141–149.

Kaur H., Attri R., Joshi J. 2016: Molecular identification of a new myxozoan, *Myxobolus dermiscalis* n. sp. (Myxosporea) infecting scales of *Labeo rohita* Hamilton in Harike Wetland, Punjab (India). Int. J. Parasitol. Parasites Wildl. 5: 139–144.

Kaur H., Katoch A., Dar S.A., Singh R. 2015: *Myxobolus nanokiensis* sp. nov. (Myxozoa: Bivalvulidae), a new pathogenic myxosporean parasite causing haemorrhagic gill disease in cultured Indian major carp fish, *Labeo rohita* (Hamilton 1822) in Punjab, India. J. Parasitic Dis. 39: 405–4013.

Ksepka S.P., Rash J.M., Whelan N., Bullard S.A. 2019: A new species of *Myxobolus* (Myxozoa: Bivalvulida) infecting the medulla oblongata and nerve cord of brook trout *Salvelinus fontinalis* in southern Appalachia (New River, NC, USA). Parasitol. Res. 118: 3241–3252

Li P., Xi B.W., Zhao X., Xie J. 2017: *Myxobolus linzhiensis* n. sp. (Myxozoa: Myxobolidae) from the gill filament of *Schizothorax oconnori* Lloyd (Cyprinidae: Schizothoracinae) in Tibet, China: morphological and molecular characterization. Parasitol. Res. 116: 3097–3103.

Li Y.C., Sato H. 2014: Two novel myxosporean species (Myxosporea: Bivalvulida), *Myxobolus marumotoi* n. sp. and *Cardimyxobolus japonensis* n. sp., from the dark sleeper, *Odontobutis obscura*, in Japan. Parasitol. Res. 113: 1371–1381.

Liu J.N., Zhang J.Y., Zhao Y.J. 2019a: Morphological and molecular characterization of a new species *Myxobolus gutturocola* n. sp. (Myxozoa: Myxobolidae) from the throat of *Hypophthalmichthys molitrix* in China. Parasitol. Res. 118: 733–781.

Liu X.O., Zhang D.D., Yang C.Z., Zhao Y.J. 2019b: Morphological and molecular identification of *Myxobolus parakoi* sp. nov. (Myxozoa, Myxobolidae) from *Cyprinus carpio* in Chongquin, China. Zootaxa 4657: 117–126.

Liu X., Hua C., Zhang Q., Zhao Y., Zhang D., Zhang J. 2017: *Myxobolus taibaiensis* sp. n. (Myxozoa: Myxosporea) infecting the intestinal wall of common carp *Cyprinus carpio* Linnaeus in China. Folia Parasitol. 64: 001.

Liu X.H., Voronin V.N., Dudin A.S., Zhang J.Y. 2016a: Morphological and molecular characterization of *Myxobolus mucosus* sp. n. (Myxosporea: Myxobolidae) with basifilamental sporulation in two cyprinid fishes, *Rutilus rutilus* (L.) and *Leuciscus leuciscus* (L.) in Russia. Parasitol. Res. 115: 1297–304.

Liu X.H., Batueva M.D., Zhao Y.L., Zhang J.Y., Zhang Q.Q., Li T.T., Li A.H. 2016b: Morphological and molecular characterisation of *Myxobolus pronini* n. sp. (Myxozoa: Myxobolidae) from the abdominal cavity and visceral serous membranes of the gibel carp *Carassius auratus* gibelio (Bloch) in Russia and China. Parasit. Vect. 9: 562.

Liu X.H., Yuan S., Zhao Y.L., Fang P., Chen H., Zhang J.Y. 2016c: Morphological and molecular characterization of *Myxobolus sheyangensis* n. sp. (Myxosporea: Myxobolidae) with intralamellar sporulation in allogynogenetic gibel carp, *Carassius auratus* gibelio (Bloch) in China. Parasitol. Res. 115: 3567–74.

Liu Y., Whipps C.M., Nie P., Gu Z. 2014: *Myxobolus oralis* sp. n. (Myxosporea: Bivalvulida) infecting the palate in the mouth of gibel carp *Carassius auratus gibelio* (Cypriniformes: Cyprinidae). Folia Parasitol. 61: 505–511.

Lövy A., Smirnov M., Brekhman V., Ofek T., Lotan T. 2018: Morphological and molecular characterization of a novel myxosporean parasite *Myxobolus bejeranoi* n. sp. (Cnidaria, Myxosporea) from hybrid tilapia in Israel. Parasitol. Res. 117: 491–499.

Lovy J., Hutcheson J.M. 2016: *Myxobolus mauriensis* n. sp. infecting rib cartilage of young-of-the-year river herring in New Jersey: notes on pathology, prevalence, and genetics. J. Parasitol. 102: 419–428.

Majumder S., Panda S., Ghosh S., Bandyopadhyay P.K. 2015: Description of a new species of *Myxobolus* Bütschli, 1882 from the *Cirrhinus mrigala* Hamilton, 1822 an edible fish of India. J. Parasitic Dis. 39: 456–460.

Marcotegui P., Martorelli S. 2017: *Myxobolus saladensis* sp. nov., a new species of gill parasite of *Mugil liza* (Osteichthyes, Mugilidae) from Samborombón Bay, Buenos Aires, Argentina. Iheringia, Sér. Zool. 107: e2017026.

Mathews P.D., Madrid R.R.M, Mertins O., Rigoni V.L.S., Morandini A.C. 2020a: A new *Myxobolus* (Cnidaria: Myxosporea) infecting the ornamental catfish *Corydoras schwartzi* from the Purus River in Brazil. Eur. J. Taxon. 620: 1–14.

Mathews P.D., Mertins O., Milanin T., Espinoza L.L., Flores-Gonzalez A.P., Audebert F., Morandini A.C. 2020b: Molecular phylogeny and taxonomy of a new *Myxobolus* species from the endangered ornamental fish, *Otocinclus coca-*

ma endemic to Peru: a host-parasite coextinction approach. Acta Trop. 210: 105545.

Mathews P.D., Maia A.A.M., Adriano E.A. 2016: Morphological and ultrastructural aspects of *Myxobolus niger* n. sp. (Myxozoa) gill parasite of *Corydoras melini* (Siluriformes: Callichthyidae) from Brazilian Amazon. Acta Trop. 158: 214–219.

Milanin T., Bartholomew J.L., Atkinson A.D. 2020: *Myxobolus* spp. (Cnidaria: Myxozoa) in introduced yellow perch *Perca flavescens* (Mitchill, 1814). Parasitol. Res. 119: 893–901.

Mohilal N., Sony T. 2017: *Myxobolus danrici* sp. n. (Cnidaria Myxosporea, Myxobolidae), a myxozoan parasite of *Esomus danrica* Hamilton, 1882 from ponds and ditches of Thoubal, Manipur, India. Bull. Pure Appl. Sci.-Zool. 36: 93–101.

Molnár K., Székely C., Guti C.F., Eszterbauer E. 2014: Two new *Myxobolus* spp. (Myxozoa: Myxobolidae) from white bream, *Blicca bjoerkna* (Linnaeus, 1758) developing in basifilamental location of gills. Acta Protozool. 53: 277–285.

Naldoni J., Carriero M.M., Moreira G.S.A., Silva M.R.M., Maia A.A.M., Adriano E.A. 2020a: Increasing the known biodiversity of cnidarian parasites of bryconid fishes from South America: two novel *Myxobolus* species with ultrastructure and ssrDNA – based phylogeny. Parasitol. Res. 19: 3627–3637.

Naldoni J., Pereira J.O.L., Milanin T., Adriano E.A., Silva M, R, M., Maia A. A.M. 2020b: Taxonomy, phylogeny and host-parasite interaction of two novel *Myxobolus* species infecting *Brycon orthotaenia* from the São Francisco River, Brazil. Parasitol. Int. 76: 102061.

Naldoni J., Zatti S.A., Silva M.R.M., Maia A.A., Adriano E.A. 2019: Morphological, ultrastructural, and phylogenetic analysis of two novel *Myxobolus* species (Cnidaria: Myxosporea) parasitizing bryconid fish from São Francisco River, Brazil. Parasitol. Int. 71: 27–36.

Naldoni J., Maia A.A.M., Correa L.L., Silva M.R.M., Adriano E.A. 2018: New myxosporeans parasitizing *Phractocephalus hemioliopterus* from Brazil: morphology, ultrastructure and SSU-rDNA sequencing. Dis. Aquat. Org. 128: 37–49.

Naldoni J., Zatti S.A., Capodifoglio K.R.H., Milanin T., Maia A.A., Silva M.R., Adriano E.A. 2015: Host-parasite and phylogenetic relationships of *Myxobolus filamentum* sp. n. (Myxozoa: Myxosporea), a parasite of *Brycon orthotaenia* (Characiformes: Bryconidae) in Brazil. Folia Parasitol. 62: 014.

Pekmezci G.Z., Yardimci B., Yilmaz S., Polat N. 2014: *Myxobolus anatolicus* sp. nov. (Myxozoa) infecting the gill of Anatolian khramulya *Capoeta tinca* (Cyprinidae) in Turkey. Dis. Aquat. Org. 109: 213–222.

Rocha S., Azevedo C., Alves Â., Antunes C., Casal G. 2019a: Morphological and molecular characterization of myxobolids (Cnidaria, Myxozoa) infecting cypriniforms (Actinopterygii, Teleostei) endemic to the Iberian Peninsula. Parasite 26: 48.

Rocha S., Casal G., Alves A., Antunes C., Rodrigues G., Azevedo C. 2019b: Myxozoan biodiversity in mullets (Teleostei, Mugilidae) unravels hyperdiversification of *Myxobolus* (Cnidaria, Myxosporea). Parasitol. Res. 118: 3279–3305.

Rosser T.G., Baumgartner W.A., Barger M.A., Griffin M.J. 2017: *Myxobolus lepomis* n. sp. (Cnidaria: Myxobolidae), a gill myxozoan infecting *Lepomis marginatus* Holbrook and *Lepomis miniatus* Jordan (Perciformes: Centrarchidae), in the Big Thicket National Preserve, Texas, USA. Syst. Parasitol. 94: 535–545.

Rosser T.G., Griffin M.J., Quiniou S.M.A., Alberson N.R., Woodyard E.T., Mischke C.C., Greenway T.E., Wise D.J., Pote L.M. 2016: *Myxobolus ictiobus* n. sp. and *Myxobolus minutus* n. sp. (Cnidaria: Myxobolidae) from the gills of the smallmouth buffalo *Ictiobus bubalus* Rafinesque (Cypriniformes: Catostomidae). Syst. Parasitol. 93: 565–574.

Saha M., Bandyopadhyay P.K. 2017: Light and scanning electron microscopic studies of *Myxobolus indica* n. sp. and a report of three Myxozoan (Myxosporea: Bivalvulida) parasites of cultured ornamental goldfish, *Carassius auratus* L. for the first time in India. Aquacul. Rep. 7: 66–76.

Stilwell J.M., Stilwell N.K., Camus A.C., Ware C., Rosser T.G., Griffin M.J. 2020a: Necroulcerative dermatitis associated with *Myxobolus dermatoulcerans* n. sp. (Cnidaria: Myxobolidae) in redbellied piranha, *Pygocentrus nattereri* Kner (Characiformes: Serrasalmidae), from Peru. Syst Parasitol, 7: 649–659.

Stilwell J.M., Petty, B.D. Camus A.C., Woodyard, E.T., Griffin, M.T., Rosser, T.G. 2020b: Characterisation of *Myxobolus stellatus* n. sp. (Cnidaria: Myxobolidae) infecting the cranial nerves and ganglia of the spotfin hatchetfish *Thoracocharax stellatus* (Kner) (Characiformes: Gasteropelecidae) from Colombia. Syst. Parasitol. 97: 305–314.

Székely C., Molnár K., Cech G. 2015a: Description of *Myxobolus balatonicus* n. sp. (Myxozoa: Myxobolidae) from the common carp *Cyprinus carpio* L. in Lake Balaton Syst. Parasitol. 91: 71–79.

Székely C., Cech G., Chaudhary A., Borzk R., Singh H.S., Molnár K. 2015b: Myxozoan infections of the three Indian major carps in fish ponds around Meerut, UP, India, with descriptions of three new species, *Myxobolus basuhaldari* sp. n., *M. kalavatiae* sp. n. and *M. meerutensis* sp. n., and the redescription of *M. catlae* and *M. bhadrensis.* Parasitol. Res. 114: 1301–1311.

Tahir U.B., Guo Q.X., Zhao D.D., Liu Y., Gu Z. 2019: Description of *Myxobolus xiantaoensis* n. sp. from the fins of yellow catfish in China: a species previously attributed to *Myxobolus physophilus* Reuss, 1906 in Chinese records. Parasitol. Res. 118: 1137–1143.

Vieira D.H.M.D., Tagliavini V.P., Abdallah V.D., Azevedo R.K. 2018: *Myxobolus imparfinis* n. sp. (Myxozoa: Myxosporea), a new gill parasite of I*mparfinis mirini* Haseman (Siluriformes: Heptapteridae) in Brazil. Syst. Parasitol. 95: 309–318.

Vieira D.H.M.D., Alama-Bermejo G., Bartholomew J.L., Abdallah V.D., Azevedo R.K. 2017: Morphological and molecular description of *Myxobolus batalhensis* n. sp. (Myxozoa, Myxosporea), a liver and ovary parasite of *Salminus hilarii* in Brazil. Parasitol. Res. 116: 3303–3313.

Voronin V.N., Duduin A.S., 2015: [The description of *Myxobolus pelecicola* sp. nov. (Myxozoa: Myxobolidae) from *Pelecus cultratus* (Cypriniformes, Cyprinidae)]. Parazitologiya 49: 257–263. (In Russian.)

Wu W., Wang Q.S., Sato H., Zhang J.Y. 2019: Morphological and molecular characterization of muscle-infecting myxosporean *Myxobolus xinyangensis* sp. nov. from *Abbottina rivularis* in China. Dis. Aquat. Org. 132: 171–179.

Xi B.W., Zhao X., Li P., Xie J. 2019: Morphological variation in *Myxobolus drjagini* (Akhmerov, 1954) from silver carp and description of *Myxobolus paratypicus* n. sp. (Cnidaria: Myxozoa). Parasitol. Res. 118: 2149–2157.

Yurakhno V.M., Ovcharenko M.O. 2014: Study of Myxosporea (Myxozoa), infecting worldwide mullet with description of a new species. Parasitol. Res. 113: 3661–3674.

Zatti S.A., Atkinson S.D., Maia A.A.M., Corrêa L.L., Bartholomew J.L. Adriano E.A. 2018: Novel *Myxobolu*s and *Ellipsomyxa* species (Cnidaria: Myxozoa) parasitising *Brachyplatystoma rousseauxii* (Siluriformes: Pimelodidae) in the Amazon basin, Brazil. Parasitol. Int. 67: 612–621.

Zatti S.A., Naldoni J., Silva M.R.M., Maia A.A.M., Adriano E.A. 2015: Morphology, ultrastructure and phylogeny of *Myxobolus curimatae* n. sp. (Myxozoa: Myxosporea) a parasite of *Prochilodus costatus* (Teleostei: Prochilodontidae) from the São Francisco River, Brazil. Parasitol. Int. 64: 362–368.

Zhang J.Y., Liu X.H., Voronin V.N., Dudin A.S., Tokarev Y.S. 2019: *Myxobolus pelecicola* Voronin et Dudin 2015 is a junior synonym of *Myxobolus ladogensis* Rumyantsev et Schulman 1997 (Myxosporea: Myxobolidae) infecting the skeletal muscle of sichel *Pelecus cultratus* (Actinopterygii: Cyprinidae) in Russia. Parasitol. Res. 118: 3099–3103.

Zhang B., Zhai Y., Liu Y., Gu Z. 2017: *Myxobolus pseudowulii* sp. n. (Myxozoa: Myxosporea), a new skin parasite of yellow catfish *Tachysurus fulvidraco* (Richardson) and redescription of *Myxobolus voremkhai* (Akhmerov, 1960). Folia Parasitol. 64: 030.

Zhang J.Y., Al-Quraishy S., Abdel-Azeem S., Abdel-Baki A.A. 2014: The morphological and molecular characterization of *Myxobolus khaliji* n. sp. (Myxozoa: Myxosporea) from the double bar seabream *Acanthopagrus bifasciatus* (Forsskål, 1775) in the Arabian Gulf, Saudi Arabia. Parasitol. Res. 113: 2177–2183.

Received 19 November 2020 Accepted 17 February 2021 Published online 25 May 2021

Cite this article as: Eiras J.C., Cruz C.F., Saraiva A., Adriano E.A. 2021: Synopsis of the species of *Myxobolus* (Cnidaria, Myxozoa, Myxosporea) described between 2014 and 2020. Folia Parasitol. 68: 012.